Title
X-RAY INDUCED X-RAY FLUORESCENCE ANALYSIS OF SUSPENDED AIR PARTICULATE MATTER

Authors
Giauque, Robert D.
Goda, Lilly Y.
Garrett, Roberta B.

Publication Date
1974-06-01

LBL-2951
UC-11
TID-4500-R61

X-RAY INDUCED X-RAY FLUORESCENCE ANALYSIS OF SUSPENDED AIR PARTICULATE MATTER

Robert D. Giauque, Lilly Y. Goda, and Roberta B. Garrett

June 1974

Prepared for the U. S. Atomic Energy Commission
under Contract W-7405-ENG-48

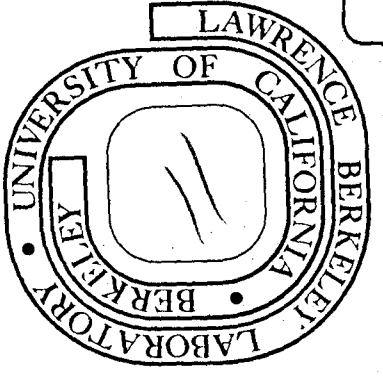

LBL-2951

DISCLAIMER

X-RAY INDUCED X-RAY FLUORESCENCE ANALYSIS OF SUSPENDED AIR PARTICULATE MATTER*

Robert D. Giauque, Lilly Y. Goda, and Roberta B. Garrett

Nuclear Chemistry Division
Lawrence Berkeley Laboratory
University of California
Berkeley, California 94720

July 1974

ABSTRACT

This report reviews critical aspects of x-ray induced x-ray fluorescence analysis that should be considered for quantitative elemental analysis of suspended air particulate matter. Included are considerations which influence sensitivity and precision in x-ray fluorescence analysis using semiconductor detector spectrometers. The analytical capabilities of spectrometers employed during these studies will be illustrated. Also, a method employed to compensate for particle size effects when analyzing for lower atomic number elements is discussed.

---

*This report was prepared as partial fulfillment of an agreement with the Rockwell International Science Center, Thousand Oaks, Calif., to participate in Phase II of the California Aerosol Characterization Experiment during 1973-1974. This program was sponsored by the California Air Resources Board. In addition to this report, approximately 550 time related aerosol specimens were analyzed by x-ray fluorescence. The program manager has been supported in analysis and interpretation of the data obtained during the study. Work performed under the auspices of the U. S. Atomic Energy Commission.

LBL-2951

INTRODUCTION

The analytical technique x-ray induced x-ray fluorescence analysis (XRF) has become a widely accepted instrumental method applicable for the elemental analysis of air particulate matter collected on filter or impactor media. Both energy and wavelength dispensive x-ray spectrometers have been employed at various laboratories to perform elemental analysis of aerosols. We will limit our discussion to the use of energy dispensive methods, since they were the methods employed during the ACHEX programs (Aerosol Characterization Experiments) sponsored by the California Air Resources Board. The analytical technique XRF is non-destructive and is illustrated in Figure 1. Exciting radiation provided by an x-ray tube or radioisotope source, either directly or indirectly, impinges upon a specimen. A fraction of the photons, if of sufficient energy, produce vacancies in the inner atomic shells of atoms within the specimen, which in turn can emit characteristic x-rays when transitions occur to fill the vacancies. In addition to these interactions, a portion of the exciting radiation is scattered either coherently or incoherently and, in turn, produces x-ray spectrum background. The x-rays are detected by a semiconductor detector and are sorted by their energies. The elemental concentrations are determined from the intensities of the individual characteristic x-rays.

SENSITIVITY FACTORS

The main conditions that determine sensitivities attainable are the x-ray peak intensities and their ratios to the background. Sensitivities are influenced by (1) selection of the excitation radiation, (2) the total system geometry, (3) the characteristics of the spectrometer employed, and (4) the choice of the substrate used to collect the aerosol specimen.

Selection of the Excitation Radiation

Although radioisotope sources have been employed to provide the exciting radiation for analyses of suspended air particulates collected on filter media,[1-3] the use of x-ray tubes directly or indirectly with secondary targets is preferable, since much higher intensity x-ray beams (typically several orders of magnitude) are obtained. Hence, higher sensitivities can be achieved by employing x-ray tubes. The use of radioisotope sources does have a slight advantage by providing essentially constant x-ray output. The output from x-ray tubes are often easily regulated to better than 1% stability over a period of 8 hours or more. This stability is more than sufficient for analyses of aerosol specimens.

For analyses of suspended air particulate matter collected on typical filter media or impactor films, the intensity of the scattered x-rays is usually quite large compared with that of the characteristic x-rays. Since conventional x-ray tubes yield a continuum of such interfering scattered radiation when employed directly to provide the exciting radiation (i.e., the scattered radiation is of the same energy as the characteristic x-rays), monochromatic exciting radiation is used. Figure 2 illustrates the spectral output one can expect from a conventional W anode x-ray tube operated at a

potential of 40 KV. Near monochromatic exciting radiation has been obtained by employing characteristic x-ray tubes.[4] Figure 3 shows the spectral output obtained from a low power (~ 20 watts) Mo transmission x-ray tube operated at a potential of 42 KV. (The combined thickness of the anode plus the window was .010 cm). Comparable exciting radiation can be attained by filtering the output from a conventional x-ray tube. Monochromatic exciting radiation can be obtained by employing x-ray tubes with secondary targets.[5] Figures 4-7 illustrate the techniques employed to provide the exciting radiation during these studies. They are discussed in detail in the appendix. The use of monochromatic exciting radiation simplifies the calibration procedures which are discussed in the section regarding calibration methods.

NOTE: A comparison of relative sensitivities attainable for two separate systems employing equal counting periods may be expressed:

$$\frac{\text{Sensitivity A}}{\text{Sensitivity B}} = \sqrt{\frac{(\text{Peak/Background})\ \text{A}}{(\text{Peak/Background})\ \text{B}}} \times \sqrt{\frac{(\text{Peak intensity})\ \text{A}}{(\text{Peak intensity})\ \text{B}}} \qquad (1)$$

where the measured x-ray peak intensity = (line-background). For example, a reduction in the peak/background ratio by a factor of 500, accompained by a reduction in the relative x-ray intensity by a factor of 10, will improve sensitivities attainable by a factor of 7.07, ($\sqrt{500/10} = 7.07$). Thus, although a modification of the primary radiation sacrifices x-ray peak intensity, the accompanying enhancement of the x-ray peak/background ratios often makes these measures advisable.

The selection of the exciting radiation energy is strongly influenced by the range of elements to be studied. Optimum sensitivity is achieved by employing an excitation radiation of energy slightly greater than the K or L absorption edge energies of the elements to be analyzed, but of sufficient energy that the incoherently scattered radiation does not produce significant overlapping background. Table I lists x-ray photoelectric cross sections (the ability to produce inner atomic shell vacancies) for selected elements for AgLα, NiKα, and MoKα x-rays. These data were obtained from tables compiled by McMaster, et al.[6] As shown, AgLα x-rays are over 100 times more efficient than MoKα x-rays for producing photoelectric interactions with the elements Al $\rightarrow$ Cl. Likewise, NiKα x-rays are approximately 10 times more efficient than MoKα x-rays for producing photoelectric interactions with the elements Al $\rightarrow$ Fe. These examples clearly illustrate that sensitivities attainable are strongly influenced by the selection of exciting radiation energy. Consequently, excitation radiation of more than one energy is employed when analyzing for a broad range of elements.

Although the fluorescent yield values (the fraction of x-rays actually emitted when transitions occur to fill inner atomic shell vacancies) are not influenced by experimental conditions, the values affect relative sensitivities attainable. Figure 8 is a plot of K and L_{III} fluorescent yield values obtained from the literature.[7,8] As shown, the fluorescent yield value of Al (0.036) and Fe (0.35) differ by an order of magnitude as there is a rapid decrease in fluorescent yield values for the lower atomic number elements.

Geometry Considerations

It is important that the excitation-specimen-detector geometry be designed for maximum practical efficiency, so that a large number of counts can be acquired in a short time. The overall geometrical efficiency shown in Figure 4 is approximately .002 (the photon intensity reaching the detector divided by the photon intensity emitted by the x-ray tube, presuming the specimen to be a perfect diffuse reflector). Although higher geometrical efficiencies can be realized by using radioisotope sources, the increase in efficiency does not compensate for the large difference in the photon output obtained from x-ray tubes, compared to the output from the typical radioisotope sources employed.

For most analyses, the intensity of the scattered x-rays is usually quite large compared with that of the characteristic x-rays from the elements in the collected aerosol specimen; hence, it is desirable that the energy loss by the incoherent (Compton) scattering process be a minimum. Figure 9 shows plots for the energy of the scattered radiation versus the energy of the exciting radiation for 90 and 180^{o} Compton scattering. As shown, the energy loss by the Compton scattering process increases with energy and with the angle of scattering.

Since the mass of the substrates used to collect the aerosol is usually quite large, compared with the mass loadings, most of the scattering is from the substrate. The intensity of the scattered radiation increases with excitation radiation energy relative to the intensity for a characteristic x-ray from any given element per unit concentration. This is due to the fact that the scattering cross section for the substrate increases relative to the photo-electric interactions produced as the energy of the excitation radiation selected increases. Figure 10 shows a plot of the fraction of the excitation radiation

scattered with respect to the total absorbed, using carbon as the scattering matrix, and, presuming absorption effects are negligible for the scattering matrix.

Spectrometer Characteristics

Progress in the electronic design of semiconductor detector spectrometers over the past five years by Goulding, et al.[9-11] has drastically improved the performance and sensitivity capabilities of semiconductor detectors. Included in these advancements was the development of guard-ring and guard-ring reject detectors which significantly reduced the x-ray spectrum background due to the loss of ionization signals in the detector. These events arise principally from high energy scattered exciting radiation which impinges upon the detector near the periphery of the sensitive region. (Goulding and Jaklevic[12] give a detailed description of processes which produce x-ray spectrum background). Comparable sensitivities can be obtained using standard type detectors by collimating down a large area detector to essentially eliminate the detection of events near the periphery of the sensitive region. Using this procedure, one obtains somewhat poorer resolution due to the higher capacitance of the larger area detector. Resolution affects sensitivities attainable and the ability to resolve x-ray signals of comparable energies. Total system resolutions of 225 eV or better at 5.9 KeV are commonplace and more than sufficient for most analyses. Count rate limitations, typically around 10,000 counts/sec,

are seldom approached with most aerosol specimens. However, analyses are performed over pre-set live times to compensate for system dead times.

Selection of the substrate

The contents, mass, and the type of loadings (surface vs. non-surface) of the substrate employed to collect the aerosol specimen very much affect sensitivities attainable. A desirable substrate should be composed entirely of low Z elements (C,H,N,O) and not contain any impurities which give rise to x-rays of energies similar to those which are to be employed for analyses. Table II lists the concentrations of impurities found in collection media employed during Phase II of the ACHEX program. As shown, the glass fiber filters contained substantial amounts of impurities. The high levels of the impurities not only produce background, but also require the x-ray tube to be operated at lower currents, due to the high intensities of x-ray lines from the filter impurities. Consequently, the concentrations of only several elements (Pb, Br, and in some cases Fe) were determined for aerosols collected using glass fiber filters. Due to the high levels of Zn in the sticky polyethylene used for the particle collections on the Lundgren impactor stages, Zn determinations were not made. The mass of the substrate used to collect the aerosol affects sensitivities attainable, since the x-ray spectrum background from the scattered exciting radiation varies, in most cases, proportionally with the substrate mass. Thus, an increase in substrate mass by a factor of 2 would lower sensitivities attainable by 40%, neglecting the contribution of air scattering. When very low mass ($\sim$ 1 mg/cm^2) substrates are employed, the contribution of the air (if present) to the total mass producing scattered exciting radiation background can be quite large (> 50%).

Substrates which collect the particulate matter on the surface, such as membrane types, are desirable when employing lower energy x-rays (< 4 KeV) for analyses. Non-surface type collection substrates give rise to absorption effects for lower energy x-rays from particles which are embedded within the substrate. Bonner, et al.[1] has reported estimated corrections for these effects when Whatman 41 Hi-Vol filters are employed.

CALIBRATION

Determination of Relative Excitation-Detection Efficiencies

Air particulate matter collected on filters (membrane type) or impactor media can be treated as "infinitely" thin specimens for most elemental analyses and, consequently, the concentration of an element is directly proportional to the intensity of one of its characteristic K or L x-ray lines. K x-rays are employed for the analysis of elements up to atomic number 56 (Ba), and L x-rays are used for the elements of higher atomic number. Ideally, one would like to have "infinitely" thin standards for each of the elements, but such is not possible. Some elements are too volatile or reactive in their elemental form (e.g. Cl, Br, I, Hg, K, Ca, Rb, Sr, Ba) or their compounds are hydroscopic. Fortunately, the relative ability to excite and detect characteristic x-rays can be calculated. This process is straightforward when monochromatic exciting radiation is employed. The intensity of an x-ray line from a "infinitely" thin specimen is directly proportional to the concentration, m_j ($\mu g/cm^2$) of the element and may be expressed:

$$I = I_o G \tau \left(1 - \frac{1}{J_{K,L}}\right) \omega_{K,L} f T \varepsilon m_j \qquad (2)$$

where I_o is the exciting radiation intensity

G is a geometry factor

τ is the photoelectric mass absorption coefficient ($\mu g/cm^2$) of the element for the excitation radiation

$J_{K,L}$ is the ratio (jump ratio) between the photoelectric mass absorption coefficients at the top and bottom of the absorption edge energy (the subscripts K or L refer to the specific energy level)

$\omega_{K,L}$ is the fluorescence yield value for the specific energy level

f is the fraction of x-ray lines of interest with respect to the total from the specific energy level

T is the fraction transmitted by the media between the specimen and the detector

ε is the detector efficiency

The values for the terms $\tau, J_{K,L}, \omega_{K,L}$, and f can be be obtained from the literature[6-8,13]. The values for T and ε may be calculated or determined with relative ease and are discussed in the Appendix. The value of $I_o G$ is determined from a single element thin film standard of known mass. We refer to the product of the terms $\tau, \left(1 - \frac{1}{J_{K,L}}\right), \omega_{K,L}, f, T, \varepsilon$, as the value K_j. Using a single element thin film standard, agreements within several percent between calculated and experimental results for K_j for eight elements have been obtained as shown in Table III. The thin film standards, of mass varying from 50-150 $\mu g/cm^2$, were prepared by K. Scheu of LBL by evaporation of the elements onto thin Al substrates (200 $\mu g/cm^2$).

Rhodes and Bonner have both reported making standards using multidrop techniques on filter media[15]. For elements with higher energy x-rays (> 15 KeV) we have prepared standards by (1) absorbing a known amount of a standard solution or cellulose powder, (2) drying the mixture, (3) weighing after an equilibration period of 24 hours, (4) pulverizing, and (5) pressing (15,000 psi) thin uniform pellets of mass 40 mg/cm^2. Using monochromatic excitation radiation, smooth curves for K_j are obtained when plotted versus absorption edge energies, as shown in Figures 11-13, for the three x-ray spectrometers employed during these studies. The drop-off in the values for K_j at the higher x-ray energies is due to the decreases in the detector efficiency, ε.

Determination of particle size effects

One problem inherent within the technique of x-ray fluorescence analysis of suspended air particulate matter is that appropriate considerations must be undertaken to compensate for particle size effects (mainly absorption effects) when analyzing for lower atomic number elements such as Al, Si, S, Cl, K, and Ca. The characteristic x-rays from these elements are low in energy, < 4 KeV, and the "infinitely" thin specimen criteria is often not valid. These elements are frequently present at above or near the $\mu g/m^3$ of air level in urban aerosols. The elements Al, Si, K, and Ca are principally present in particles > 1μ in diameter. Surface type collection substrates such as membrane filters should be employed to collect the aerosols when analyzing for these elements.

Figure 14 illustrates the problem of particle size effects using an exaggerated single particle. The exciting and fluorescent x-rays are attenuated (absorption effects) as they pass through the particle. (Inter-element enhancement effects are generally minor for analysis of air particulate matter). In reality, air particulate matter is a heterogeneous specimen, in which particles of varying shapes and composition exist. Rhodes and Hunter[16] have derived formulae to compensate for particle size effects in specimens of "non-infinite" thickness (particles not infinitely thick for exciting or characteristic radiations). The specimen is treated as being in the form of a monolayer with particle sizes of either discrete values or continuous distributions. The formulae consist of equations for a thin homogeneous specimen, multiplied by a grain size dependent factor. However, to this date, no experimental proof has been reported to substantiate the capabilities of the published formulae to adequately compensate for particle size effects for analyses of air particulate matter. One of the principal problems is that the size distribution of the collected particles is seldom known. Whitby has reported that atmospheric particulate matter usually has a bimodal mass distribution.[17] Both modes can be approximated by log-normal distribution. The large particle mode occurs at sizes varying from 5 to 50μ. These particles, in general, are principally from mechanical processes, such as wind-blown soil dust. The mass mean diameter of the larger particle mode can vary considerably with changing meteorological conditions. The larger particles, $> 40\mu m$, which are few in number, are usually not collected due to non-ideal sampling conditions. Moreover, the efficiency to collect the particles $\leq 40\mu m$ can be strongly influenced by meteorological conditions. Bounce off and wall losses have occurred for these particles using a modified Lundgren cascade impactor during

the ACHEX program. Hence, analyses of particles in the larger particle mode are often concerned with the smaller size fractions of this mode. These facts illustrate the problem of describing the distribution of the collected particle sizes.

In the approach we have employed to compensate for particle size effects, we presume the larger suspended particles are collected in the form of a monolayer. This is a reasonable assumption (particularly for larger particles) for most aerosol specimens when only several hour collection times are employed using flow rates of less than 1 cubic meter/hour/cm^2 of collection media. Also, we assume the particles are collected on the surface of the filter (membrane type) and that the particle sizes are of "non-infinite" thickness for the energies of radiations employed. (Infinite thickness is the thickness beyond which an increase in thickness would not measurably increase fluorescent x-ray line intensities). The characteristic x-ray intensity (I_c) from a given element in a homogeneous particle of average mass thickness ($\bar{m}$), gm/cm^2, may be expressed

$$I_c = I_{thin} \frac{\left[1 - e^{-(\mu_e + \mu_f)\bar{m}}\right]}{(\mu_e + \mu_f)\bar{m}} \qquad (3)$$

where I_{thin} = the characteristic x-ray line intensity from an equal amount of the particle distributed "infinitely" thin (no absorption effects), μ_e and μ_f are the total mass absorption coefficient, cm^2/gm, of the particle for the exciting and the characteristic radiation, respectively. The absorption correction term is dependent upon the total mass absorption coefficient of the particle for the exciting and characteristic radiation.

The value of the term, μ_e, and, in turn, the value of $\mu_e + \mu_f$ can be varied considerably by varying the energy of the excitation radiation. By selecting the excitation radiation (monochromatic) of energies, for which the values for μ_e vary from large to small - relative to μ_f, information on the particle size (presuming the values for μ_e and μ_f are known) can be determined; since the values of the elemental concentration obtained from I_{thin} should be the same in each case.

These larger particles which come principally from mechanical processes such as wind-blown soil dust are considered to consist of specific minerals[18]. Table IV lists these minerals. Recognizing the fact that the total mass absorption coefficients ($\mu_e + \mu_f$) of the minerals are similar when analyzing for Si (Si is usually not present as SiO_2 except in the desert region)[18] or Al, we use this to our advantage. Table IV lists the values of $\mu_e + \mu_f$ of these minerals when ZrL, AgL, or NiK x-rays are employed in excitation for the Si or Al analysis. The relationship between the mass concentration, m_1 and m_2, of an element (uncorrected for absorption effects), determined by employing two separate measurements using two different energies of excitation radiation, may be described:

$$\frac{m_2}{m_1} = \frac{1-e^{-(\mu_{e_2} + \mu_f)\bar{m}}}{1-e^{-(\mu_{e_1} + \mu_f)\bar{m}}} \times \frac{\mu_{e_1} + \mu_f}{\mu_{e_2} + \mu_f} \qquad (4)$$

where μ_{e_1} and μ_{e_2} are the total mass absorption coefficients of the particle for the two different excitation radiation energies, respectively, and $\bar{m}$ is the average mass thickness of the particle (gm/cm^2).

By setting a value $r = (\mu_{e_2} + \mu_f)/(\mu_{e_1} + \mu_f)$, equation 5 may be written:

$$\frac{m_2}{m_1} = \frac{1-e^{-r(\mu_{e_1} + \mu_f)\bar{m}}}{r\left(1-e^{-(\mu_{e_1} + \mu_f)\bar{m}}\right)} \tag{5}$$

The total mass concentration from a total of n particles may be expressed:

$$m = \sum_{i=1}^{n} m_i \left[\frac{(\mu_e + \mu_f)m_i}{1-e^{-(\mu_e + \mu_f)m_i}}\right] . \tag{6}$$

Since the mass concentration is independent of the energy of the excitation radiation employed (presuming infinite thickness is not attained for any of the individual particles), the value for $(\mu_e + \mu_f)\bar{m}$ may be determined and, in turn, the value of m is ascertained. Although this procedure requires that a weighted average value for $\bar{m}$ be employed, the net error in the result is relatively small. This is due to the fact that the bulk of the mass concentration is usually within a relatively small range, since the total mass of a particle can vary as the cube of the particle diameter.

Figure 15 shows curves for selected "r" values which could be employed for Si mass determinations with Zr and AgL x-rays plotted versus the absorption correction term to be applied, to correct for absorption effects, for the analysis with AgL x-rays. For our experiments, we employed an "r" value of 1.55. The value of the absorption correction term for the Si analysis of particles collected on the total filters was typically in the range of 1.5 to 3.0. This corresponds to particles approximately in the 8 to

24 μ size range (for unit density spheres). These are reasonable values considering the Whitby data[17] and the fact that non-ideal sampling conditions are employed. We make an additional Si determination, using NiK x-rays for excitation, to verify that we have selected close to the appropriate values for the mass absorption coefficients to ascertain the value of the absorption correction term. The total mass absorption coefficients of the minerals typically present in the aerosols are very similar for the Si and Al determinations. Consequently, the value of the absorption correction term established for the Si analysis is applied for the Al determination.

ACKNOWLEDGMENTS

We are indebted to D. Malone for designing the low-energy x-ray spectrometer. The authors with to express gratitude to S. Wright, J. Walton, N. Madden and W. Searles for fabricating and testing the equipment. We are grateful to J. Anderson and D. Malone for constructing the low-energy spectrometer. We have profited from discussions and consultations with J. Jaklevic. Appreciation is expressed to F. Goulding, J. Jaklevic, and other members of the Nuclear Instrumentation Group for developing and supplying much of the equipment used. N. Brown and D. Gok have assisted in developing the data analyses programs employed. The authors especially want to thank G. Hidy of the Rockwell International Science Center for supporting our efforts in the ACHEX programs sponsored by the California Air Resources Board. We thank J. Hollander for his encouragement in this work. The authors are grateful to J. Wesolowski and B. Appel of the California Department of Public Health for their support and cooperation in this work.

REFERENCES

1. N. A. Bonner, F. Bazan, and D. C. Camp, Lawrence Livermore Laboratory, Livermore, California, Report UCRL-51388 (1973).

2. J. R. Rhodes, A. H. Pradzynski, and R. D. Sieberg, Anal. Instrum. 10, 143-150 (1972).

3. J. A. Cooper, Nucl. Instrum. and Methods, 106, 525-538 (1973).

4. J. M. Jaklevic, R. D. Giauque, D. F. Malone, and W. L. Searles, Advances in X-ray Analysis, 15 266-275 (1972).

5. F. S. Goulding and J. M. Jaklevic, Report to the Environmental Protection Agency, EPA Report No. EPA-R2-73-182 (1973).

6. W. H. McMaster, N. K. Del Grande, J. H. Mellett, and J. H. Hubbell, Lawrence Livermore Laboratory, Livermore, California, Report UCRL-50174, Section II, Revision I (1969).

7. W. Bambynek, B. Craseman, R. W. Fink, H. U. Freund, H. Mark, C. D. Swift, R. E. Price, and P. Venugopala Rao, Rev. of Mod. Phys. 44, No. 4, 716-813 (1972).

8. E. J. McGuire, Phys. Rev., A3, 587 (1971).

9. F. S. Goulding, J. Walton, and D. F. Malone, Nucl. Inst. Methods, 71, 273-279 (1969).

10. D. A. Landis, F. S. Goulding, R. H. Pehl, and J. T. Walton, IEEE Trans. Nucl. Sci. NS-18, No. 1, 115-124 (1971).

11. F. S. Goulding, J. M. Jaklevic, B. V. Jarrett, and D. A. Landis, see Ref. 4, 470-482.

12. F. S. Goulding and J. M. Jaklevic, Ann. Rev. of Nucl. Sci. 23, 45-74 (1973).

13. G. G. Johnson, Jr., and E. W. White, ASTM DS 46, Am. Soc. Testing Mater. (1970).

14. R. D. Giauque, F. S. Goulding, J. M. Jaklevic, and R. H. Pehl, Anal. Chem. 45, 671-681 (1973).

15. D. C. Camp, J. A. Cooper, and J. R. Rhodes, X-Ray Spectrom. 3, 47-50 (1974).

16. J. R. Rhodes and C. B. Hunter, X-Ray Spectrom, 1, 113-117 (1972).

17. K. T. Whitby, Univ. of Minnesota, Minneapolis, Minnesota, Particle Tech. Lab. Pub. No. 218 (1973).

18. E. L. Kothny, California Department of Public Health, Berkeley, Calif. private communication, 1973.

Table I. Photoelectric Cross Sections

Excitation radiation	AgLα	NiKα	MoKα
Element			
Al	720 cm^2/gm	62 cm^2/gm	4.9 cm^2/gm
Si	880	80	6.4
S	1200	113	9.4
Cl	1280	132	11
K		179	16
Ca		207	19
Ti		243	23
V		268	25
Cr		304	29
Mn		328	32
Fe		363	37
Ni			47
Cu			49
Zn			55
As			65
Se			68
Br			74
Rb			82
Sr			87

Table II. Collection Media Impurities

	Washed Gelman GA-1 filters	Sticky polyethylene	Glass Fiber filters
Concentration	$\mu g/cm^2$	$\mu g/cm^2$	$\mu g/cm^2$
Element			
K	-	-	43±5
Ca	0.170±0.010	-	41±4
Fe	0.029±0.002	0.015±0.003	2.6±0.2
Cu	0.023±0.003	-	-
Zn	0.004±0.001	0.06±0.01	167±8
Rb	-	-	0.41±0.04
Sr	-	-	17±1
Ba	-	-	139±20
Pb	-	-	0.22±0.02

Table III. Relative Excitation and Detection Efficiencies (K_j)

Line	Calculated	Determined
CrKα	.381	.370±.011
MnKα	.450	.435±.003
FeKα	.587	.559±.003
NiKα	.884	.882±.007
CuKα	1.000	1.000±.015
AsKα	1.653	1.660±.083
SeKα	1.776	1.753±.057
PbLα	.804	.774±.019

Table IV. Total Mass Absorption Coefficients (cm^2/gm)

Excitation radiation	ZrL		AgL		NiK	
Element of interest	Al	Si	Al	Si	Al	Si
Mineral						
Kaolinite $Al_2(Si_2O_3)(OH)_4$	2450	2540	1620	1710	1240	1330
Anorthite $CaAl_2Si_2O_8$	2540	2680	1660	1800	1280	1430
Microline $KAlSi_3O_8$	2520	2390	1620	1490	1240	1110
Albite $NaAlSi_3O_8$	2790	2630	1820	1660	1370	1200

FIGURE CAPTIONS

Fig. 1. Schematic of x-ray fluorescence analysis technique.

Fig. 2. Generalized spectral output obtained from a conventional W anode x-ray tube operated at a potential of 40 KV.

Fig. 3. Spectral output obtained from a Mo transmission x-ray tube operated at a potential of 42 KV.

Fig. 4. X-ray fluorescence analysis technique employing direct excitation using a Mo transmission x-ray tube.

Fig. 5. X-ray fluorescence analysis technique using a W anode x-ray tube and three secondary targets to provide the exciting radiation (Goulding - Jaklevic, E.P.A. type x-ray spectrometer).

Fig. 6. X-ray fluorescence analysis technique employing a Ag anode x-ray tube and three secondary targets to provide the exciting radiation.

Fig. 7. X-ray fluorescence analysis technique employing direct excitation using a Ag anode x-ray tube.

Fig. 8. "Fitted" fluorescence yield curves for the K and L_{III} energy levels.

Fig. 9. Scattering curves for 90 and 180^{O} Compton scattering.

Fig. 10. Scattering to total cross section curve for carbon matrix.

Fig. 11. Relative excitation - detection efficiency curves for MoK x-rays.

Fig. 12. Relative excitation-detection efficiency curve for TbK x-rays.

Fig. 13. Relative excitation-detection efficiency curve for AgL x-rays.

Fig. 14. Exaggerated illustration of particle size effects for a single particle.

Fig. 15. Absorption correction curves for Si mass determinations.

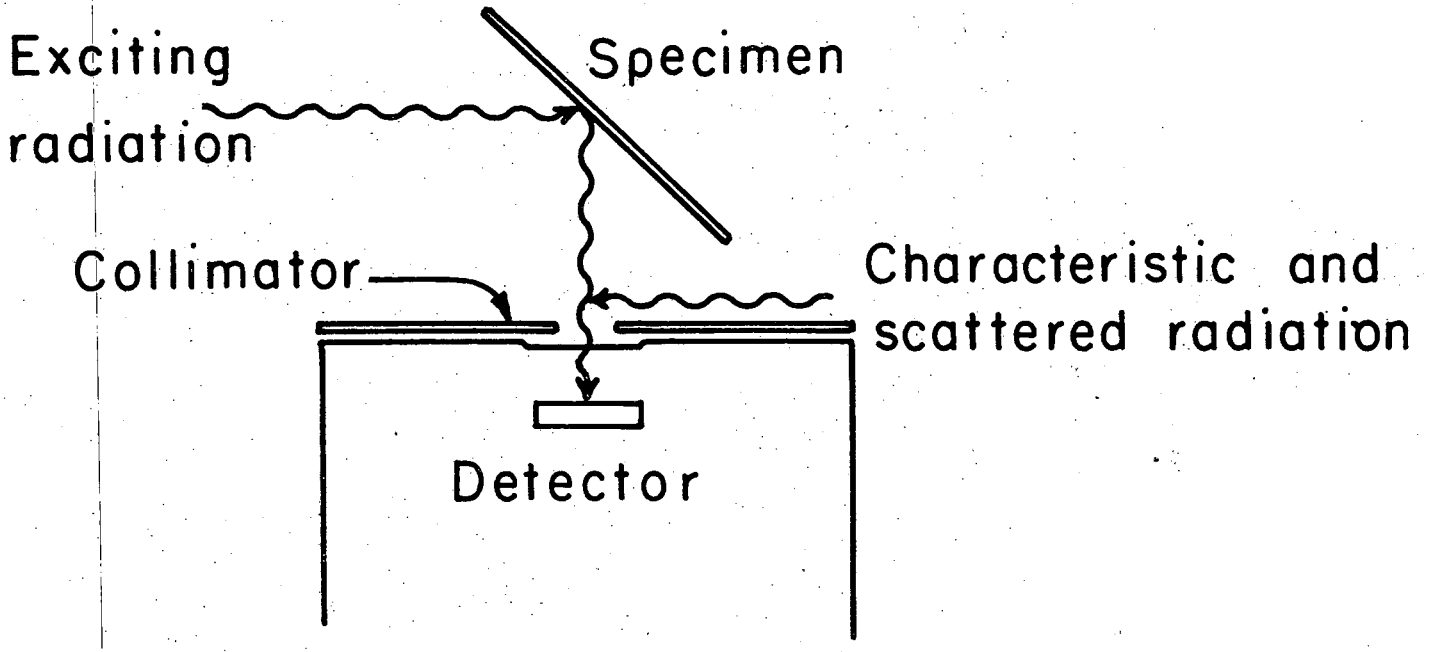

XBL747-3764

Fig. 1

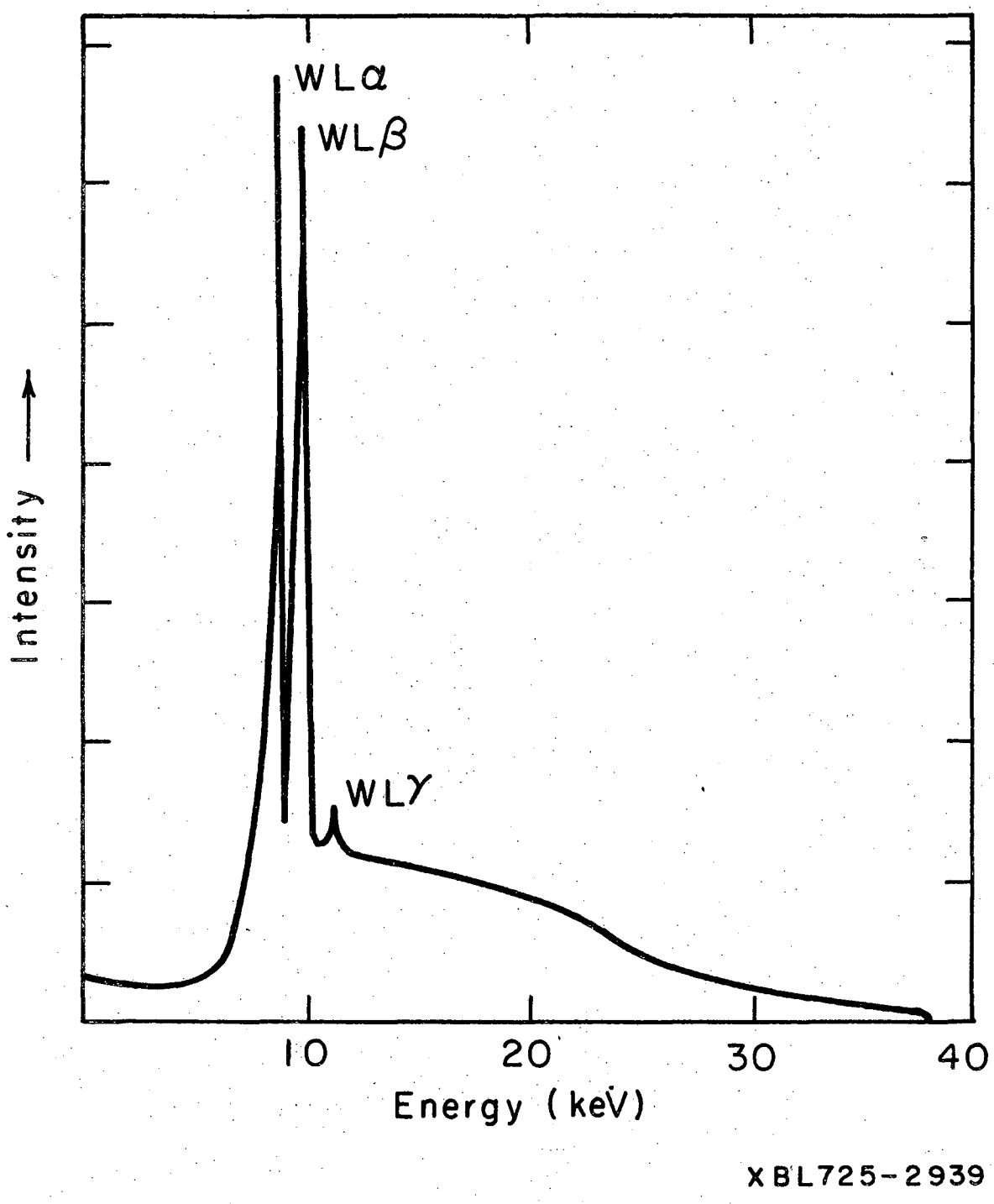

Fig. 2

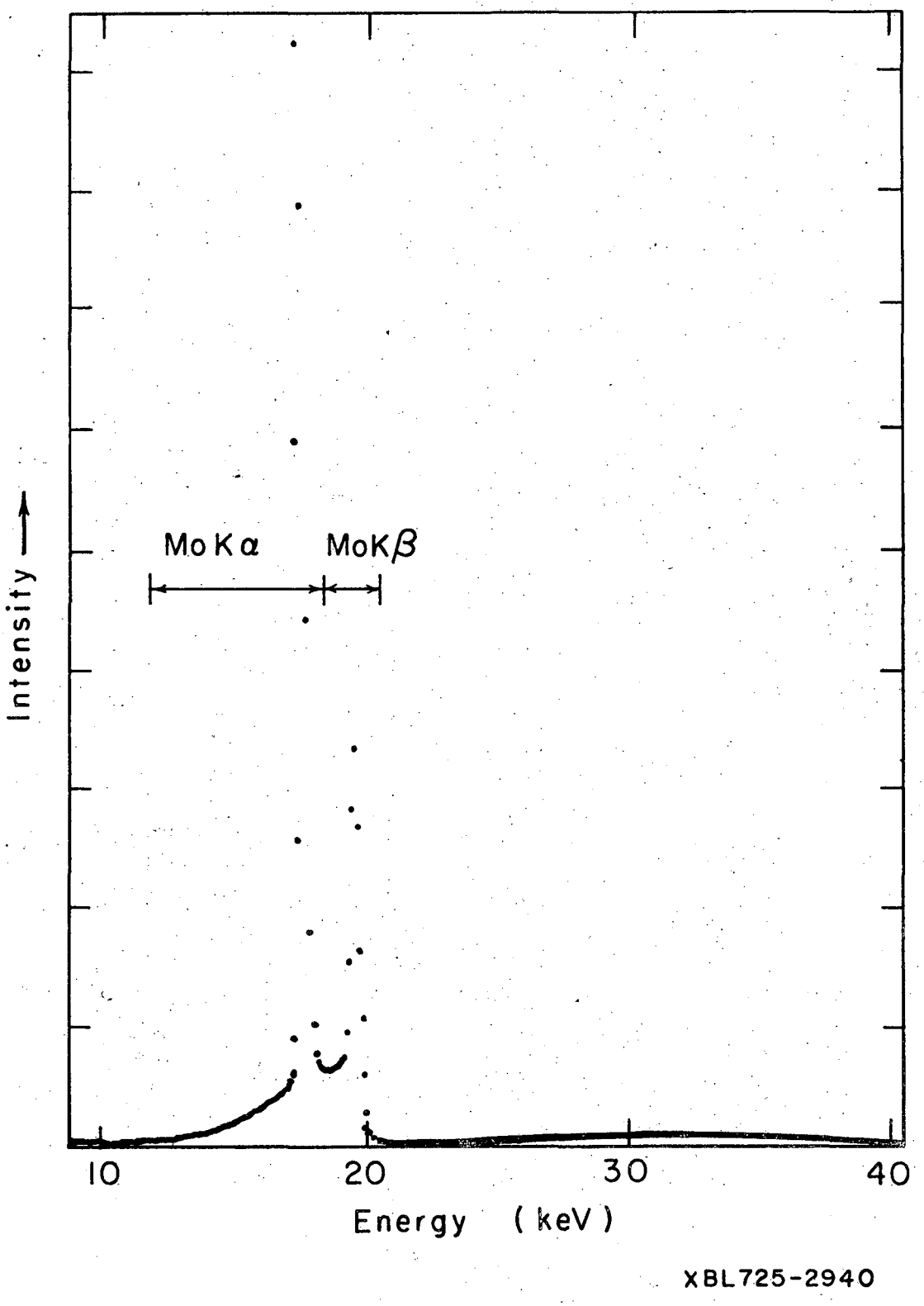

Fig. 3

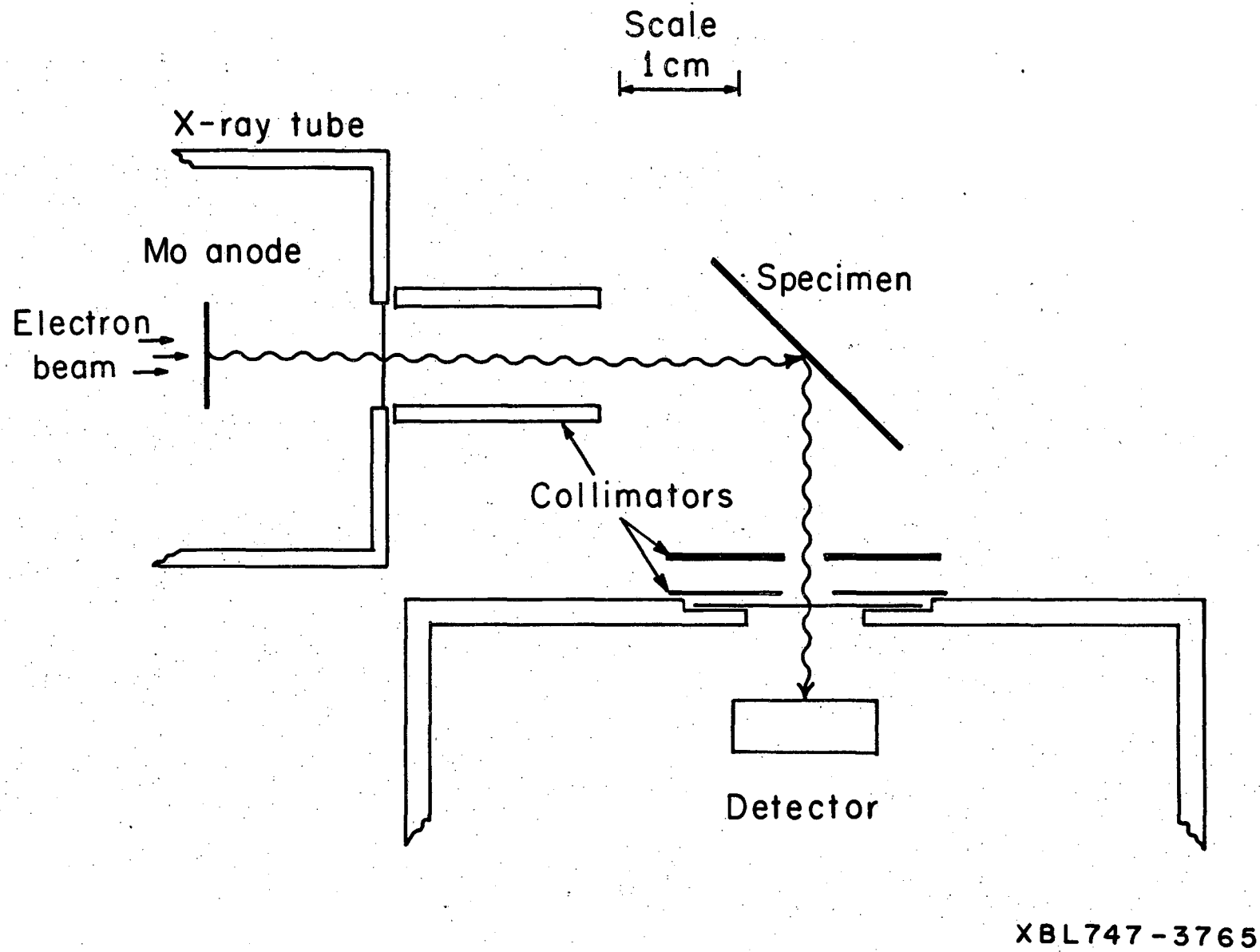

Fig. 4

LBL-2951

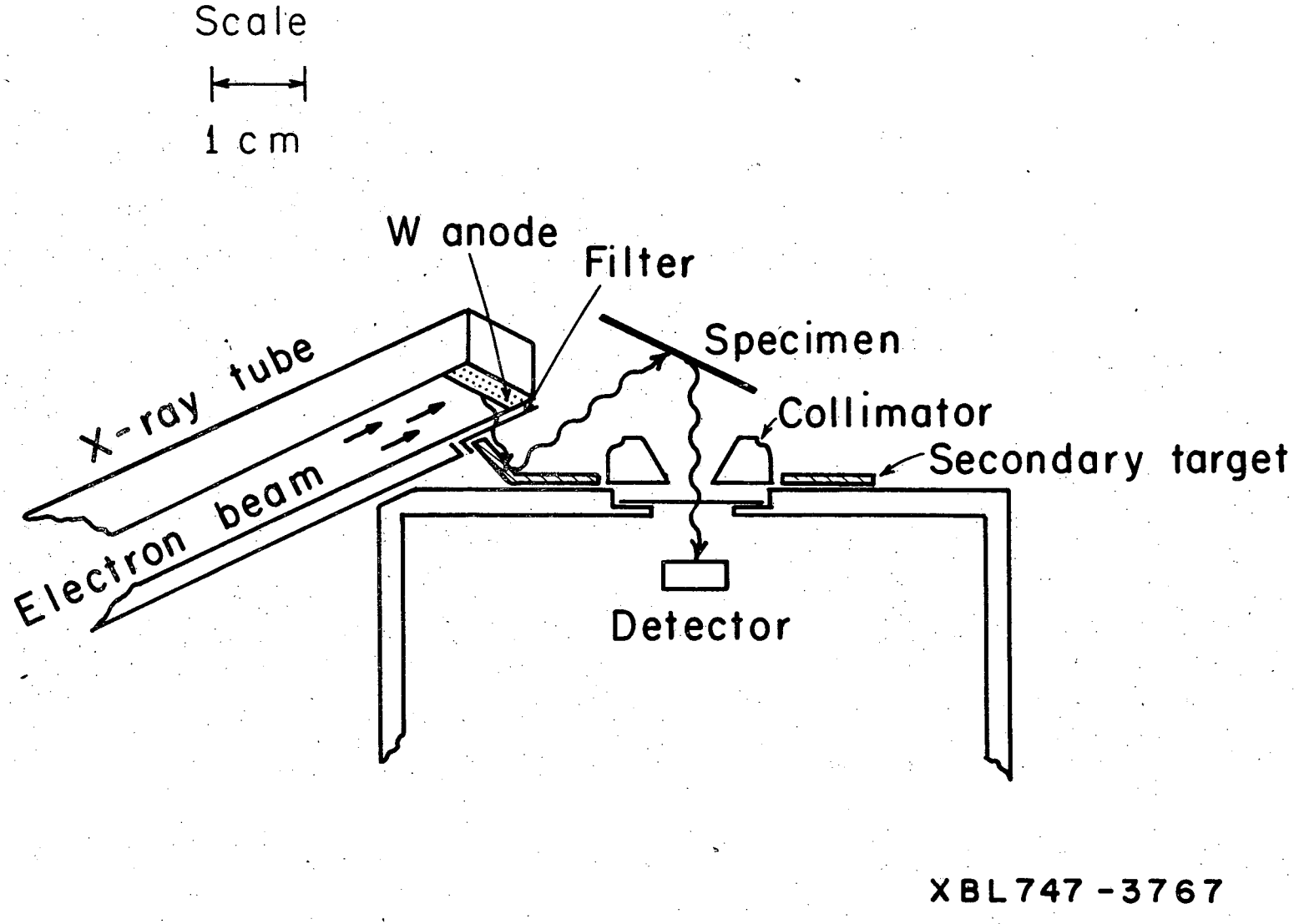
Scale
1 cm
W anode
Filter
Specimen
X-ray tube
Collimator
Secondary target
Electron beam
Detector
XBL747-3767

Fig. 5

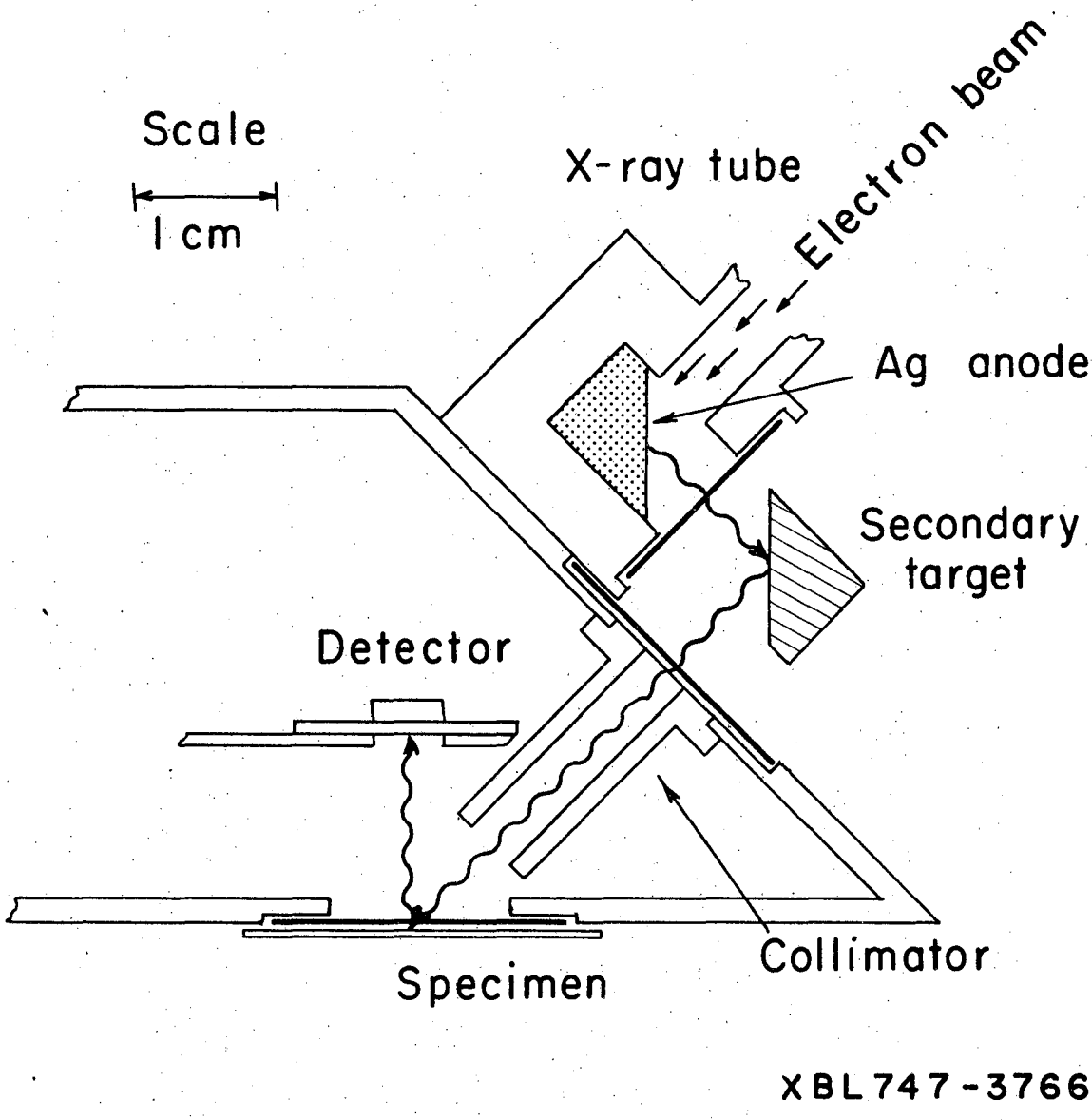
Scale
1 cm
X-ray tube
Electron beam
Ag anode
Secondary target
Detector
Specimen
Collimator
XBL747-3766

Fig. 6

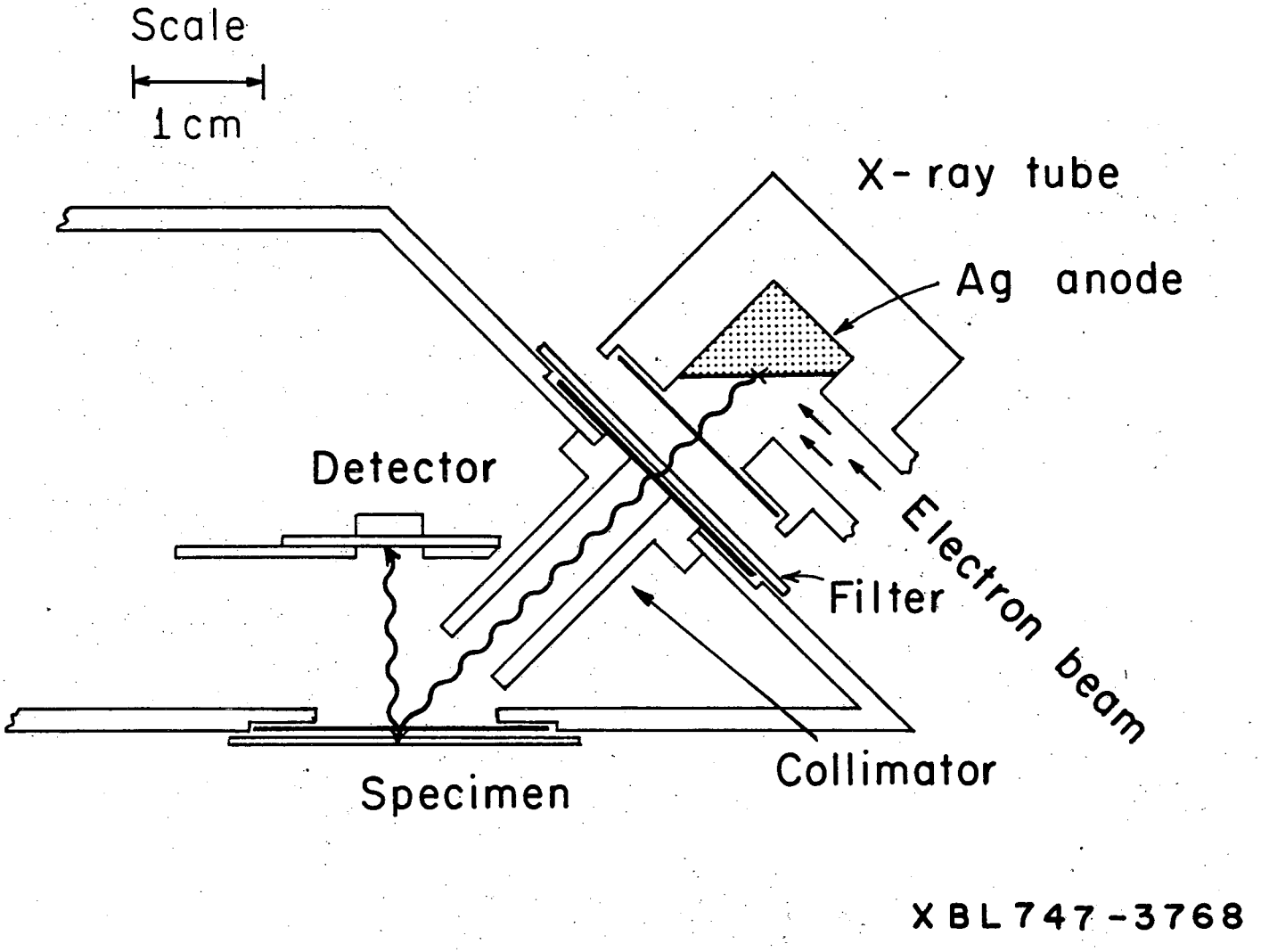
Scale
1 cm
X-ray tube
Ag anode
Detector
Electron beam
Filter
Collimator
Specimen
XBL747-3768

Fig. 7

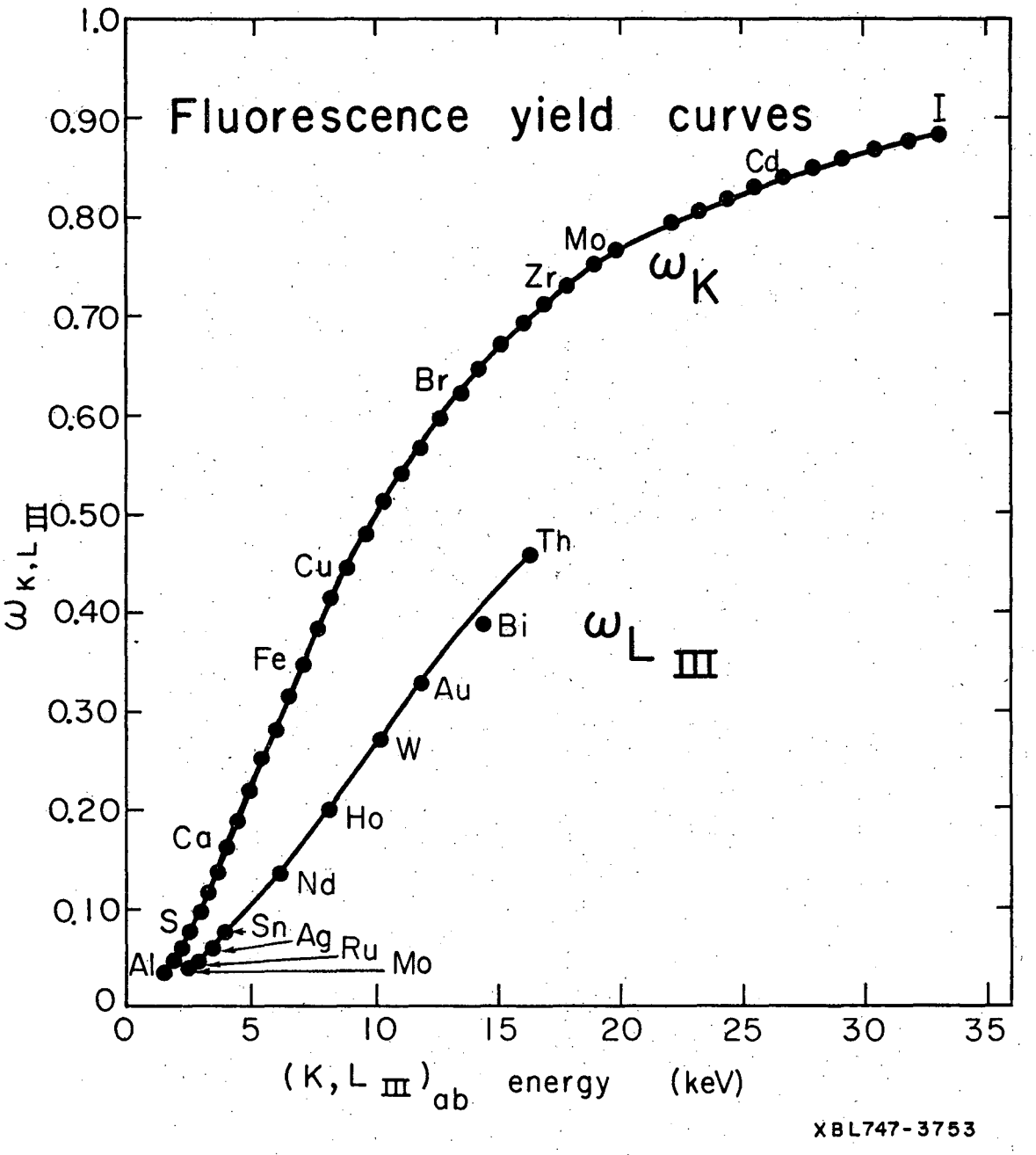
Fluorescence yield curves
I
Cd
Mo
Zr
ω_K
Br
Th
Cu
Bi
$\omega_{L\ III}$
Fe
Au
W
Ho
Ca
Nd
S
Sn
Ag
Ru
Mo
Al
$\omega_{K,L\ III}$
1.0
0.90
0.80
0.70
0.60
0.50
0.40
0.30
0.20
0.10
0
0
5
10
15
20
25
30
35
$(K, L_{III})_{ab}$ energy (keV)
XBL747-3753

Fig. 8

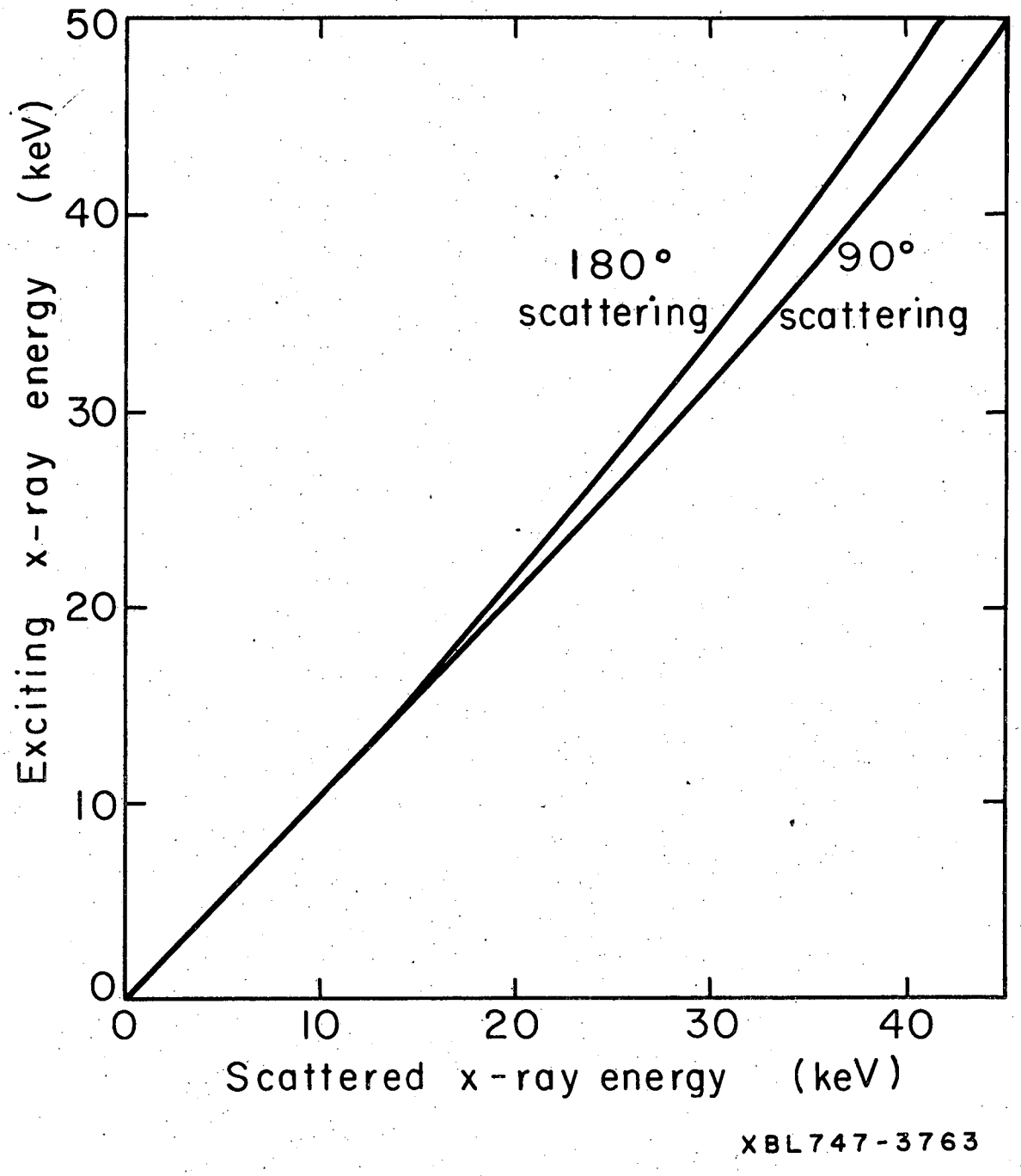
50
40
30
20
10
0
Exciting x-ray energy (keV)
180°
scattering
90°
scattering
0
10
20
30
40
Scattered x-ray energy (keV)
XBL747-3763

Fig. 9

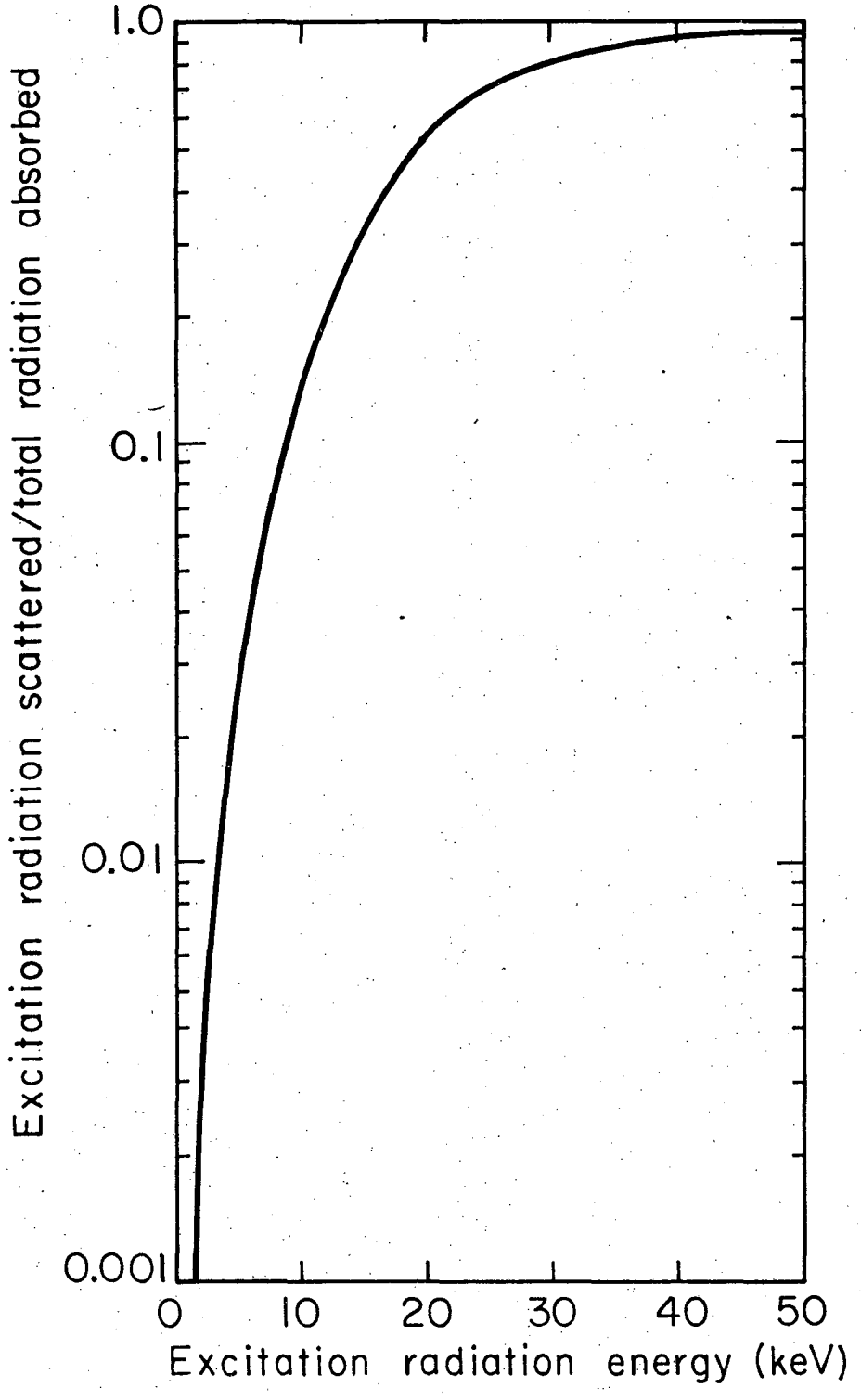
1.0
0.1
0.01
0.001
Excitation radiation scattered/total radiation absorbed
0
10
20
30
40
50
Excitation radiation energy (keV)
XBL747-3762

Fig. 10

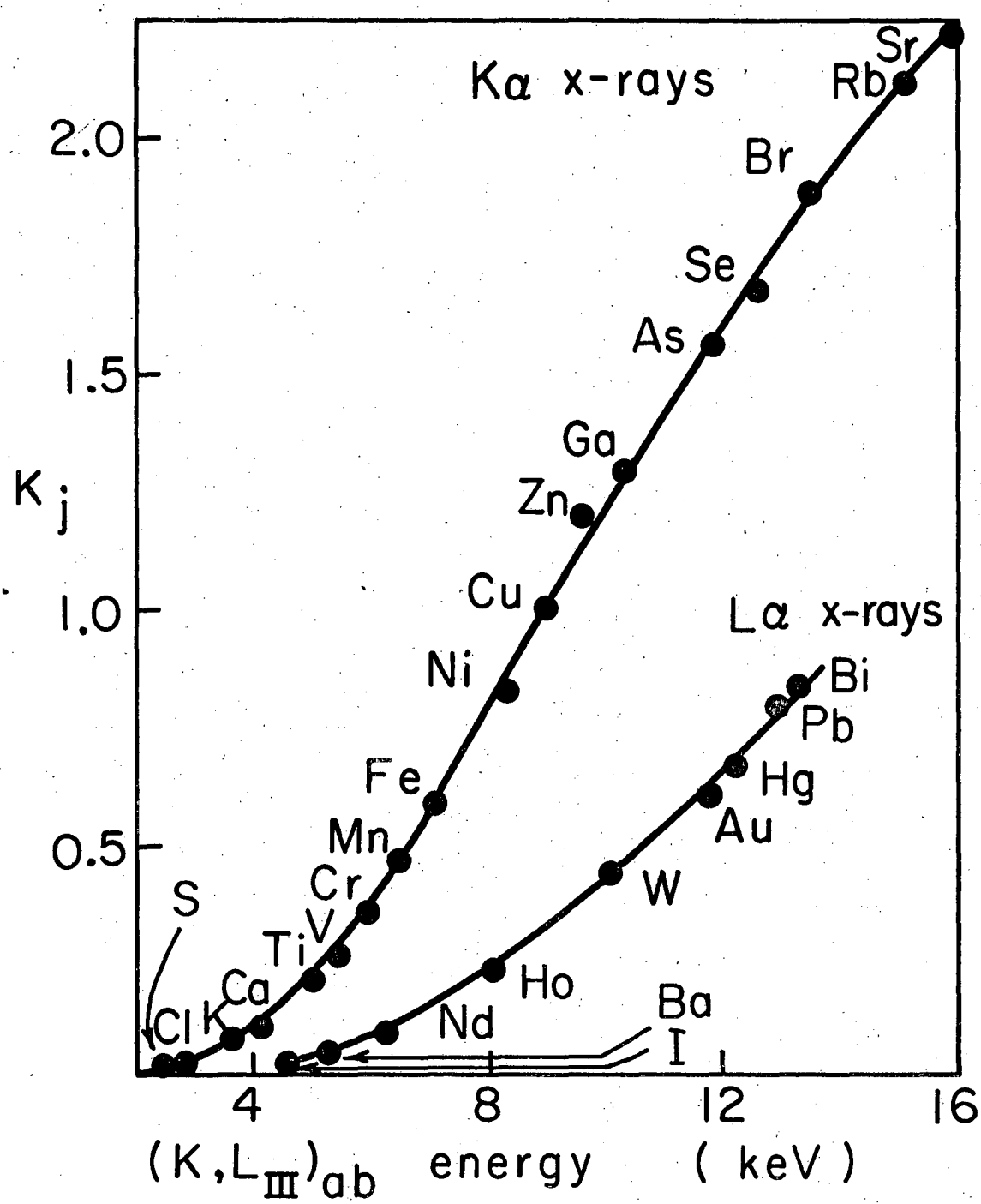
Kα x-rays
Lα x-rays
Sr
Rb
Br
Se
As
Ga
Zn
Cu
Ni
Fe
Mn
Cr
V
Ti
Ca
K
Cl
S
Bi
Pb
Hg
Au
W
Ho
Nd
Ba
I
2.0
1.5
1.0
0.5
K_j
4
8
12
16
$(K, L_{III})_{ab}$ energy (keV)
XBL747-3755

Fig. 11

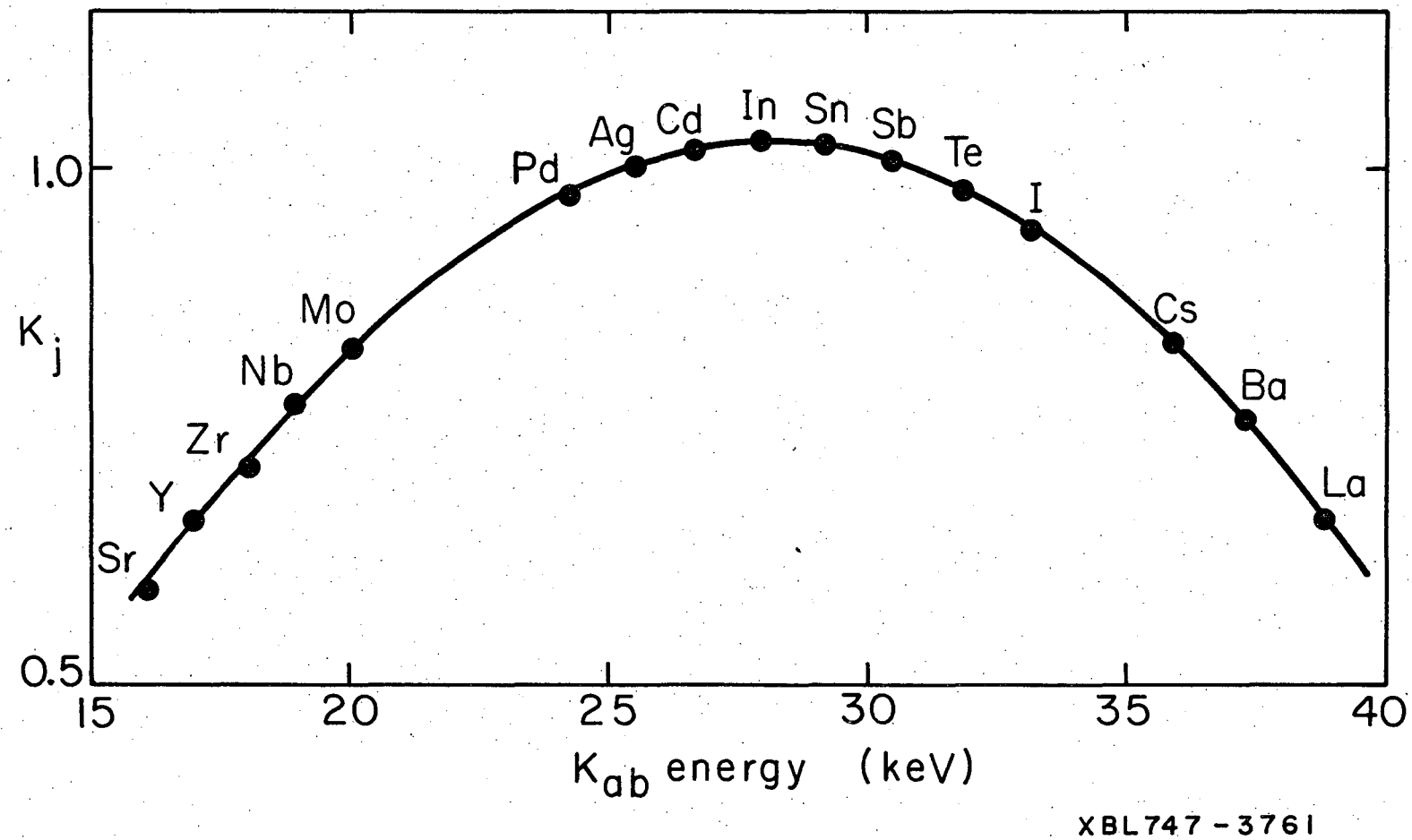
1.0
0.5
K_j
Sr
Y
Zr
Nb
Mo
Pd
Ag
Cd
In
Sn
Sb
Te
I
Cs
Ba
La
15
20
25
30
35
40
K_{ab} energy (keV)
XBL747-3761

Fig. 12

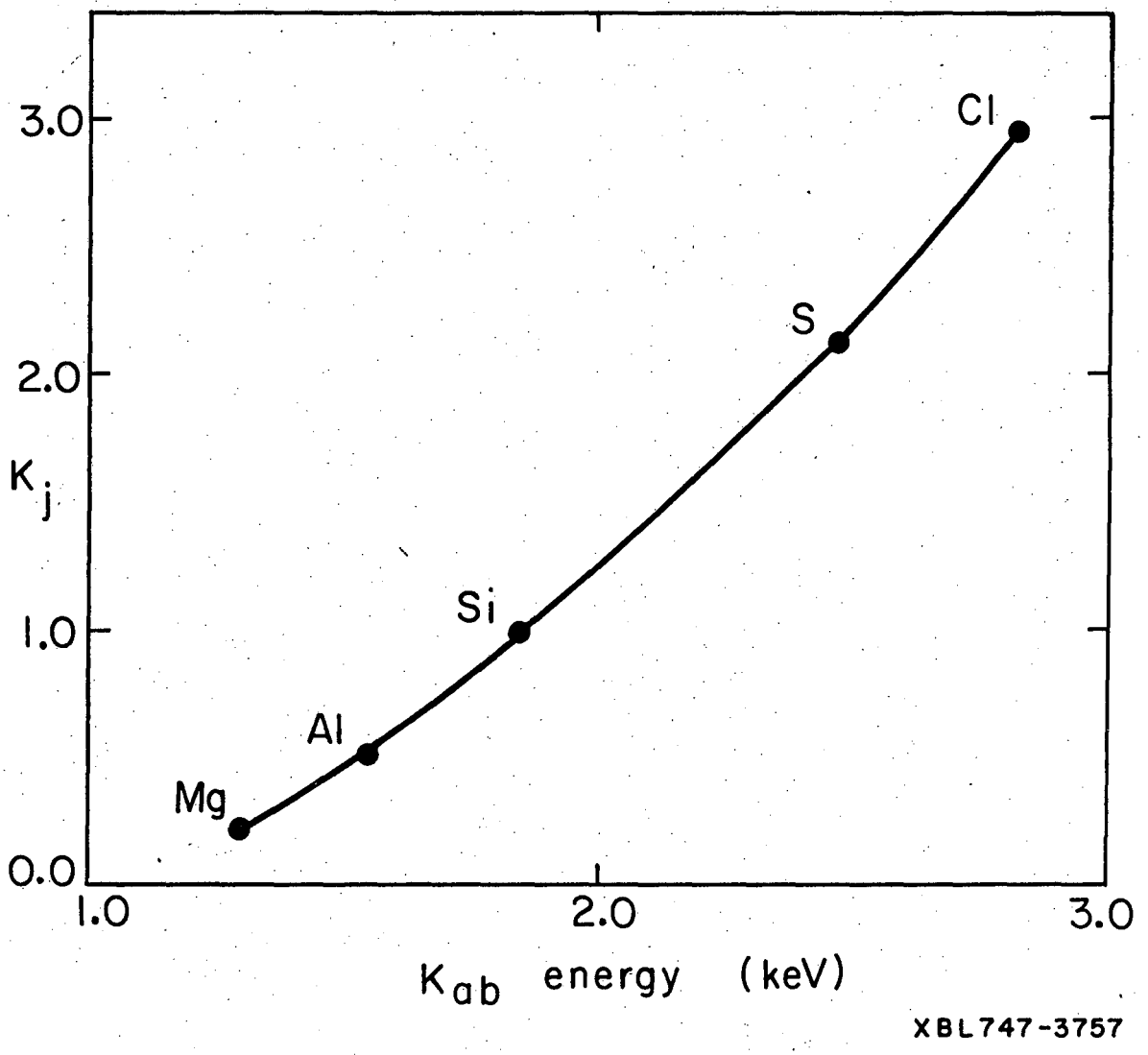

Fig. 13

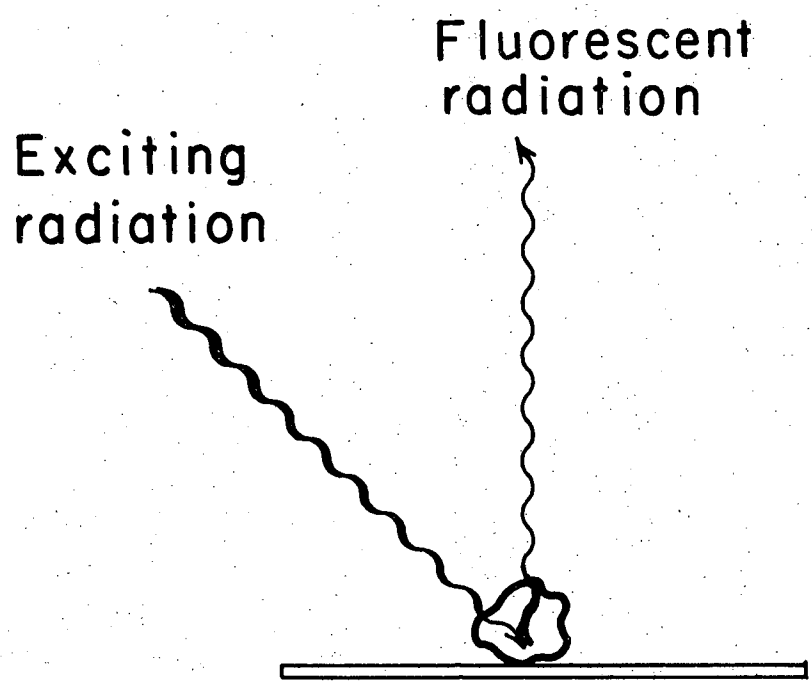

XBL747-3758

Fig. 14

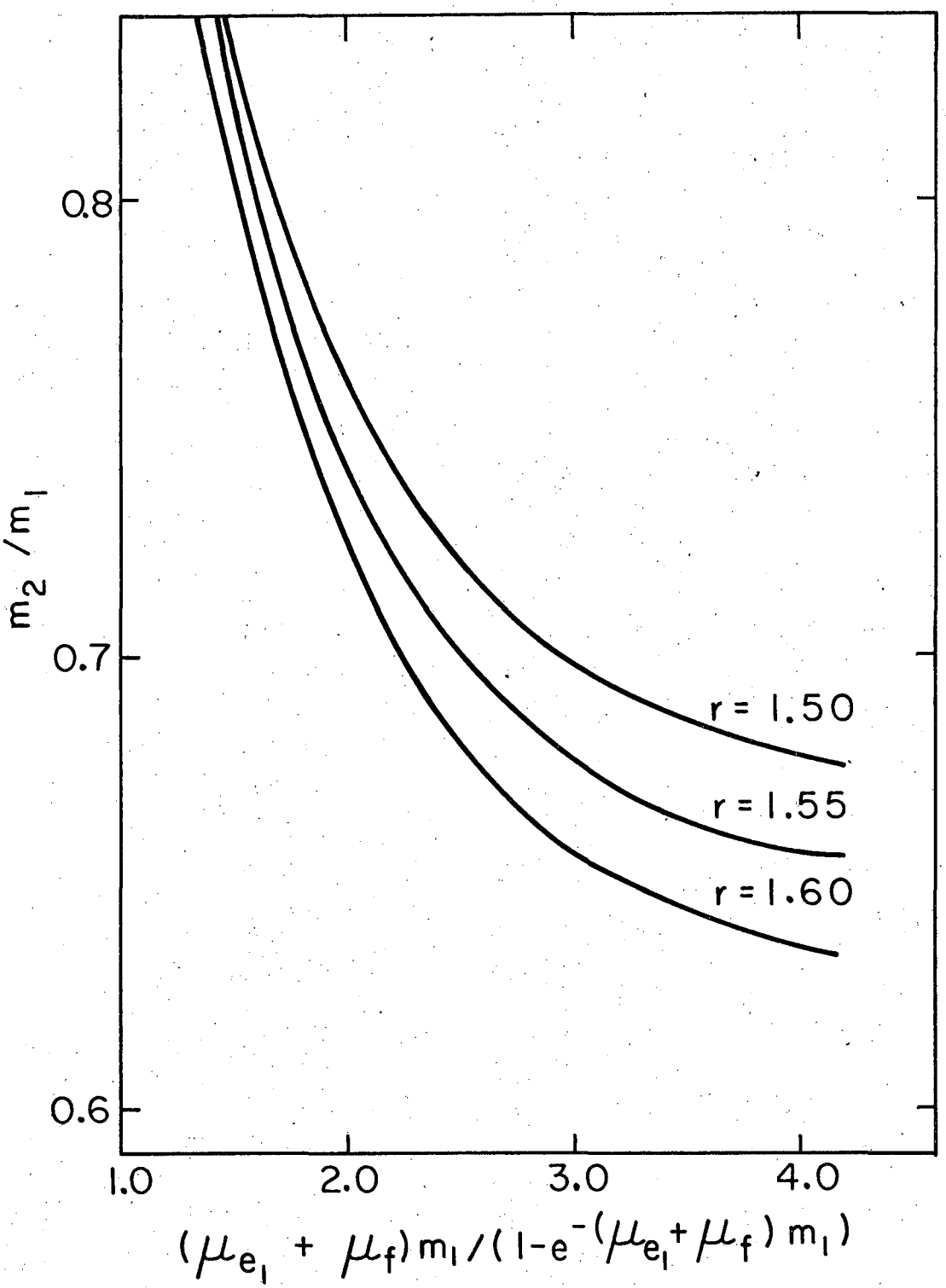

XBL747-3756

Fig. 15

APPENDIX

In this section, factors which affect the accuracy of the method are discussed. Included are considerations undertaken to standardize the three x-ray spectrometers used during these studies. Also, methods employed for the analyses program are described.

Equipment and Characteristics

Table V lists the characteristics of the x-ray spectrometers and associated x-ray tubes employed during these studies.

Standardization of spectrometers

a) Spectrometer with Mo transmission x-ray tube.

This spectrometer, A, is illustrated in Fig. 4. The procedure used to standardize this equipment has been previously reported.[14] The principal sources of error in the standardization procedure employed are from the uncertainties of (1) the fluorescent yield "fitted" values selected, and (2) the corrections employed to compensate for air absorption for lower energy x-rays. This spectrometer was employed to obtain most of the data acquired during these studies. Table VI lists the sensitivities (3 σ values) for the elements determined using 10 minute analyses times. The uncertainty in the "fitted" fluorescent yield values employed was typically 5% or less for the elements V $\rightarrow$ Sr. The uncertainty in the fluorescent yield values for the elements S $\rightarrow$ Ti was larger, attaining a maximum of 14% for S. Each day a single element thin film standard, Cu, was used to normalize for geometry and x-ray tube output. The corrections applied in the calculations to correct for air absorption of the S, K, and Ca x-rays were .34, .68, and .75, respectively. The uncertainties in these values were approximately .02 for S, .01 for K, and .01 for Ca. Figure 16

shows a spectrum obtained on a two hour total filter aerosol specimen (5 mg/cm^2 Gelman cellulose ester substrate). The elemental values listed are in ng/cm^2.

b) Spectrometer with W anode x-ray tube and three secondary targets (Ni, Mo, and Tb).

This spectrometer, B, designed by F. Goulding and J. Jaklevic,[5] is illustrated in Figure 5. Although this spectrometer has a broad range of analysis capabilities (S → Ba, Hg, Pb), it was employed only to determine the concentrations of higher Z elements which we could not obtain with spectrometer A. Somewhat higher sensitivities were attainable with spectrometer A for the elements S → Zn (compared to spectrometer B, Mo secondary target), due to the smaller contribution to the spectrum background from air scattering. Table VII lists the sensitivities (3 σ values) obtained for the elements determined using a Tb secondary target and 10 minute analyses times. Figure 17 shows a spectrum obtained on a Hi-Vol aerosol specimen. The elemental values listed are in ng/cm^2. Standardization of this spectrometer was accomplished using cellulose pellet standards. (Calculated values were not employed, due to the more complex overall geometry of this system which made it difficult to determine the detector efficiency for any given x-ray energy). Each standard was prepared by absorbing a known amount of a standard solution on cellulose powder, drying, weighing, and pulverizing the mixture from which 40 mg/cm^2 pellets were pressed. Measurements to compensate for absorption effects within the pellets were made.[14]

c) Low Energy x-ray spectrometer with Ag x-ray tube.

This spectrometer, C, shown in Figure 6 and 7, was designed by D . Malone.

The spectrometer was constructed to support research on extending the analytical technique of x-ray induced x-ray fluorescence analysis of aerosol specimens to include the determination of lower Z elements (Mg → Cl). This unique spectrometer permitted compact excitation-specimen-detector geometries to be obtained. Additionally, a short path length, 1.5 mm, between the specimen and the detector window was attained. Either air or He paths could be used. In the secondary target mode (Fig. 6), three targets, Zr, Ag, and Ni, were utilized to obtain data which permitted us to compensate for particle size effects as previously discussed. Sensitivities for most of these elements were enhanced substantially when the x-ray tube output was employed directly (Fig. 7) to provide the exciting radiation, using only a .00025 cm Ag filter to attenuate the Bremstrahlung. Figure 18 shows a spectrum acquired in this mode. The concentrations listed are in ng/cm^2. Table VIII lists the sensitivities attainable in each of the modes using 10 minute analyses times. Using the particle size information acquired for the Si analyses in the secondary target mode, the Mg and Al x-ray intensity data obtained in the direct mode are corrected to compensate for particle size effects.

An infinitely thick pure Si disk was employed to standardize this spectrometer. The mass of an infinitely thick (mass absorption coefficient term ~4) may be expressed:

$$m_{inf} = 0.98/(\mu_e \csc\phi_e + \mu_f \csc\phi_f) \qquad (7)$$

where ϕ_e and ϕ_f are the angles formed by the exciting and the fluorescent radiation with the disk surface.

Since a pure disk of this mass will suffer a 75% loss in x-ray intensity (the product of the attenuation of the exciting and characteristic x-rays integrated

over the mass, $m_{inf.}$), the mass of the standard for calibration purposes equals $m_{inf.}/4.0$. We have employed this same procedure to standardize for Al and S and obtained agreements to within 5% of the calculated relative excitation-detection efficiency values normalized to Si. For these calculations, corrections are applied to compensate for the detector dead layer (equivalent surface mass for which ionization events are not measured) and for absorption by the very thin Au layer on the surface of the detector. For this spectrometer, these attentuation corrections for Mg → Ca K x-rays were in the range of 5 to 15%.

Data Analysis Program

X-ray spectra of the collected areosol specimens are acquired using a 512 channel pulse-height analyzer and are recorded on magnetic tape. The analytical computations are made by a Control Data 6600 computer. Although our program has been established for the analyses of many types of specimens, much less than 50K of core space would actually be required for analyses of aerosols only. The analysis program is performed in three steps. First, the x-ray spectrum background due to the scattered exciting radiation is removed, secondly, the interferences due to overlapping x-ray lines are unfolded, and thirdly, the concentrations of the elements in the original air samples are calculated from the intensities of the appropriate x-ray lines employed for analysis.

The shape of the scattered exciting radiation background is simply determined by employing a blank filter of mass similar to that of the filters used for the aerosol collections. The scattered x-ray background within various energy ranges to be employed for analysis are ratioed to the intensity of the scattered exciting radiation. These scattered radiation background

factors are employed for analyses. This procedure was possible since the typical aerosol loadings contributed only a couple of percent to the total mass of the filter plus collected aerosol.

Fixed sets of channels corresponding to preselected energy ranges are employed for analyses. Although the spectrometer is stable over widely varying conditions, one of the more intense x-ray lines is used to compensate if a base-line shift occurs. To obtain high statistical accuracies, between 70 to 80 percent of the total peak areas are utilized for analyses. The peak fractions used are established from elemental thin-films. Corrections for overlapping x-ray lines are also determined from the elemental thin-films by establishing relationships between individual peak shapes and intensities. In effect, a series of simultaneous equations are established which compensate for overlapping x-ray lines occurring over preselected energy ranges.

The concentrations of the individual elements present in the aerosol are then calculated from the individual x-ray line intensities using Eq. (8).

$$\frac{\mu g_j}{m^3} = \frac{c_j}{c_s} \times \frac{m_s}{V} \times \frac{1}{K_j} \qquad (8)$$

where c_j and c_s are the characteristic x-ray count rates from element j and the standard

m_s is the standard mass ($\mu g/cm^2$)

V is the volume of air sampled (m^3) per cm^2 of collection media

K_j is the relative excitation-detection efficiency value normalized to the standard

Discussion of Sources of Analytical Errors

We have observed losses between 5 and 50% of elements present in the larger particles (> 5μ) due to specimen handling techniques. Such losses have occurred between x-ray fluorescence analysis (XRF) and neutron activation analysis. Upon reanalysis by XRF, agreement, typically within 5%, is obtained from small particle elements (Pb and Br), while low values are obtained from large particle elements (Ca, Ti, and Fe). Also, large particle element losses have been observed for the aerosol specimens, cut and stored in envelopes, prior to analysis with the low-energy spectrometer. Potential handling losses appear to be related to the size of the particles and to the relative humidity at the time of collection.

Due to the compact excitation-specimen-detector system geometries employed, it is essential that fixed reproducible geometries be obtained. For example, an incorrectly seated specimen, located 0.6 mm away from the plane of the correct position, relative to the detector, for spectrometer A, would yield results which were 20% low. The problem is accentuated since the spectrometer was designed to have the center lines of the excitation and the detector systems intersect at the specimen plane. However, we have been able to reproduce our results (analyses performed several months apart), typically within 4%, which substantiates the fact that we do obtain reproducible geometries.

A second geometrical error can arise from the fact that the probability of exciting and detecting an x-ray line from the aerosol varies over the area of the specimen analyzed. Figure 19 illustrates the relative intensity of an x-ray line from various parts of the specimen area employed for analysis with spectrometer A.

The total area of the specimen analyzed was 3 cm^2. For analyses, we presume that the aerosol is deposited uniformly across the filter surface. For the Lundgren impactor stages, the size of the x-ray beam spot is reduced such that only a 1 cm^2 area is examined. For stages 1 and 2 ($\sim$ 12μ 50% cut point), appreciable errors (> 20%) can be obtained due to the fact that the uniform deposit criteria is not valid.

Additionally, losses, due to bounce-off (using sticky polyethylene surface) and entrainment within the impactor, have been observed for elements present princially in the large particles (> 5μ). The losses are related to the relative humidity at the time the aerosol is collected. Losses up to 50% have been determined by comparing the data from the sum of the stages from the Lundgren impactor and the after filter with the total filter data.

Thin-films are prepared to determine overlapping x-ray lines by establishing relationships between individual x-ray peak shapes and relative intensities. These thin-films are prepared either by dusting the finely pulverized element or element compound onto mylar tape, or by evaporation onto thin backings, such as aluminum or polyamide. The masses of these thin films are unimportant as long as the relative difference for absorption of the x-rays is negligible. Table IX lists the major overlapping x-ray lines determined during the ACHEX program.

X-rays detected by semiconductor detectors often produce peaks that tail on the low energy side. This tailing effect becomes more pronounced with increasing x-ray energy and can cause overlapping of x-ray lines, particularly when trying to discern x-rays of low intensity adjacent to a high-intensity higher energy peak. Additionally, escape peaks can be a consideration. The energy of an escape peak corresponds to the original x-ray

energy minus the energy of the escaping photons, which in the case of silicon detectors are the Si K x-rays. The intensity of the escape peaks, although energy dependent, are more than two orders of magnitude less than the initial x-ray intensity. To illustrate the magnitude of the problem of the tailing effect for spectrometer A, a Pb concentration of 1 $\mu g/cm^2$ produces a tailing background equivalent to 5, 4, 3, and 2 ng/cm^2 for the V, Cr, Mn, and Ni analyses, respectively. Thus, for analyses of minor constituents within the aerosol, it is imperative that corrections for tailing background from major constituents such as Pb, Br, and Fe be made in the data analysis program. The corrections for overlapping x-ray background due to peak tailing or escape peak are established with relative ease from the thin-films.

As previously mentioned, fixed sets of channels corresponding to preselected energy ranges are employed for analyses. A minor gain shift can occur in the energy spectrum if the spectrometer and its associated electronics are not maintained in a relatively constant temperature environment. Such gain shifts can produce sizeable errors in the results obtained for minor constituents (particularly in the higher energy range of the x-ray spectrum) having large overlapping x-ray backgrounds, using our data analysis program. Minor gain shift problems can be prevented by daily checking preselected energy ranges for x-ray lines near the two extremes of the energy spectrum and making a very minor electronic amplifier adjustment if necessary. However, we maintain our spectrometer in a relatively constant environment and consequently, adjustments are infrequently required.

X-rays from substrate impurities which are partially absorbed in the substrate can produce minor errors in the results, using our data analysis program, if the aerosol loading of the impurity elements are small compared to the blank, and if substrates of widely varying masses are employed to collect

the aerosols. Although a change in substrate mass will proportionally alter the x-ray spectrum background due to the scattered exciting radiation for spectrometers A and B, the x-ray line intensity from a substrate impurity may not be proportionally altered in intensity due to substrate absorption effects. During the ACHEX program, substrate masses were maintained relatively constant, ± 10%. The only reported element for which this problem would be a source of error is Ca for the after filter data.

Corrections for absorption effects due to aerosol loadings are not included in our analysis program. For nearly all of the analyses performed on two hour aerosol specimens collected during the ACHEX program, such absorption effects would be negligible or very minor. For example, a 100 $\mu g/cm^2$ hydrocarbon deposit mixed uniformly with a 10 $\mu g/cm^2$ $NH_4(SO_4)_2$ deposit would attenuate the SK x-rays by only 1%. A silicate deposit completely covered by a 100 $\mu g/cm^2$ hydrocarbon deposit would attenuate the SiK x-rays by only 4%. Thus, absorption effects due to aerosol loadings are minor, particularly compared to particle size effects.

Even though membrane type (Gelman GA-1 5μ cellulose ester) filters were employed to collect the total and the after filter aerosol specimens, a fraction of the very small particles will have some penetration depth into the filter medium. During the ACHEX program the particulate sulfur was determined in most cases to be predominantly present in the particles < 0.5 μ. Penetration of the particles into the filter media can cause absoprtion effects for the SK x-rays. We have determined that the sulfur containing particles have been deposited to a depth corresponding to less than 0.7 mg/cm^2. This evaluation was made by employing the low-energy spectrometer shown in Fig. 6. Sulfur

determinations were made employing both AgL and NiK x-rays for the exciting radiation. (Attentuation of NiK x-rays by the filter is essentially negligible, while the same condition is not true for the lower-energy AgL x-rays). Such a penetration depth requires less than a 10% correction for filter attenuation effects of the exciting radiation when AgL x-rays are employed for analysis in this 45° excitation-specimen geometry. Our conclusions are further substantiated from the fact that essentially identical results were obtained when AgL and NiK x-rays were employed to determine S levels on dry mylar impactor surfaces (from ACHEX I). Although we have not evaluated the attenuation effects of the filter medium for SK x-rays, we believe such effects would be minor (compared to the attenuation of the AgL x-rays) in our 180° specimen-detector geometry.

In our method to compensate for particle size effects, we assume that the larger particles originate from mechanical processes such as wind-blown soil dust. In turn, we use overall average mass absorption coefficient data, which are similar in value for a number of common minerals, for both the Si and the Al analyses. We determine the Si concentration employing two separate measurements using excitation radiation of two different energies. The mass values determined (uncorrected for particle size effects) are applied to determine the value of an absorption correction term. This approach is reasonable for the Si analyses if a large fraction of the Si is not present as SiO_2. An error of 4% in the value of the ratio of the two mass determinations established can, in turn, introduce an error of 20% for the value of the absorption correction term, ascertained for particles around 15μ (for unit density spheres). Additionally, if the selected "r" value employed is off by 3%, an additional 10 to 20% error is introduced. However, we make an additional Si determination

using NiK x-rays for excitation to verify that we have chosen the appropriate values for the mass absorption coefficients, and in turn, the correct "r" values. This is possible since the mass values (corrected for absorption effects) ascertained should be the same for all three determinations.

Although we have prepared a comprehensive list of potential sources of errors, with appropriate considerations, analyses for a broad range of elements can be accomplished to a relatively high degree of accuracy. Employing x-ray induced x-ray fluorescence analysis techniques, we have obtained data (not limited to aerosol specimens) which have usually been in good agreement ± 5-10%, with data obtained by other techniques (i.e., see Ref. 14). Table X lists the elements determined by XRF during the ACHEX II program. Additionally, the concentration and the particle size range, in which these elements were typically found, are listed. Those elements listed in brackets were determined to be only occasionally present in the aerosol specimens. In a separate report to be compiled at the Rockwell International Science Center, the extensive data obtained by XRF during this program will be discussed. The data are being combined with a wealth of other chemical, physical, and meteorological data obtained by other experiments during this study. The principal objectives of the experiment are (1) to characterize the respirable and visibility degrading fraction of aerosols in the Los Angeles South Coast Basin, (2) to investigate the evolution of aerosols under conditions of photochemical smog formation, (3) to estimate the primary and secondary aerosol contributions to the total airborne particulate concentration, (4) to evaluate the significance of both natural and anthropogenic sources in the evolution of the respirable and visibility degrading fractions of the aerosol, and (5) to recommend from the data obtained key considerations for a control strategy.

Table V

	Spectrometer A	Spectrometer B	Spectrometer C
Detector	Grounded guard-ring	Guard-ring reject	Top-hat
Electronics	Pulsed-light feedback	Pulsed-light feedback	Pulsed-light feedback
Resolution at 5.9 KeV	~ 225 eV	~ 190 eV	~ 175 eV
X-ray tube, power	Mo transmission 20 watts	W, 50 watts	Ag, 50 watts
Excitation method	Direct	Secondary targets	Direct and secondary targets

Table VI. Theoretical Limits of Detection, Spectrometer A

Media	Gelman GA-1	Sticky polyethylene
Mass (mg/cm^2)	5.0	5.0
Air volume sampled (m^3/cm^2)	0.75	2.40
Area analyzed (cm^2)	3	1
Element and spectral line		
SKα	900 ng/m^3	480 ng/m^3
ClKα	420	220
KKα	140	100
CaKα	65	55
TiKα	26	19
VKα	21	15
CrKα	17	10
MnKα	12	8
FeKα	13	10
NiKα	5	5
CuKα	8	5
ZnKα	5	12
GaKα	4	5
AsKα	5	4
SeKα	5	4
BrKα	7	5
RbKα	10	8

continued

Table VI. continued

Media	Gelman GA-1	Sticky polyethylene
SrKα	12	9
HgLα	9	7
PbLα	9	7
PbLβ	23	19

Table VII. Theoretical Limits of Detection, Spectrometer B

Tb Secondary Target

Media	Whatman-41
Mass (mg/cm^2)	9.0
Air volume sampled (m^3/cm^2)	3.0
Area Analyzed (cm^2)	4
Element and spectral line	
SrKα	17 ng/m^3
YKα	16
ZrKα	14
NbKα	12
MoKα	11
PdKα	10
AgKα	9
CdKα	10
InKα	12
SnKα	13
SbKα	13
TeKα	14
IKα	17
CsKα	28
BaKα	38
LaKα	56

Table VIII. Theoretical Limits of Detection, Spectrometer C

Media	Gelman GA-1			
Mass (mg/cm^2)	5.0			
Air volume sampled (m^3/cm^2)	0.75			
Area analyzed (cm^2)	1			
Mode	Zr secondary target	Ag secondary target	Ni secondary target	Direct, Ag filter
Element and spectral line				
MgKα	-	-	-	320 ng/m^3
AlKα	900	1400	7200	130
SiKα	560	700	3500	70
SKα	-	400	1400	40
ClKα	-	370	900	40
CaKα	-	-	200	-
TiKα	-	-	130	-
FeKα	-	-	120	-

Table IX. Major Overlapping X-ray Lines

Element and spectral line	Interference
AlKα	BrL
SKα	PbM
ClKα	PbM, SKβ
CaKα	KKβ
TiKα	BaLα, FeKα escape peak
VKα	TiKβ, BaLβ, FeKβ escape peak
MnKα	FeKα
NiKα	FeKβ
GaKα	ZnKβ, PbLl
AsKα	PbLα
SeKα	PbLn
RbKα	BrKβ

Table X. California Urban Aerosols

Particle diameter	> 1μ	< 1μ
Conc. range ($\mu g/m^3$)		
> 1	Al, Si, Ca, Fe	S, Pb
0.1 - 1	K, Ti, Zn, (S)	Ca, Fe, Br (K)
0.01 - 0.1	Cr, Mn, Br, Sr, Pb (Ba)	Ti, Ni, Cu, Zn, (V) (As) (Sn) (Sb) (I)
0.001- 0.01	Ni, Cu (Ga) (Rb)	Mn (Se) (Cd)

FIGURE CAPTIONS

Fig. 16. Spectrum of a total filter aerosol specimen collected over a two hour interval.

Fig. 17. Spectrum of a Hi-Vol aerosol specimen collected over a 24 hour period.

Fig. 18. Spectrum of a total filter aerosol specimen collected over a two hour interval.

Fig. 19. Relative intensity of CuK x-ray line from various parts of the specimen area employed for analysis. These data were obtained using the Mo transmission x-ray tube and a 2 mm x 2 mm Cu specimen.

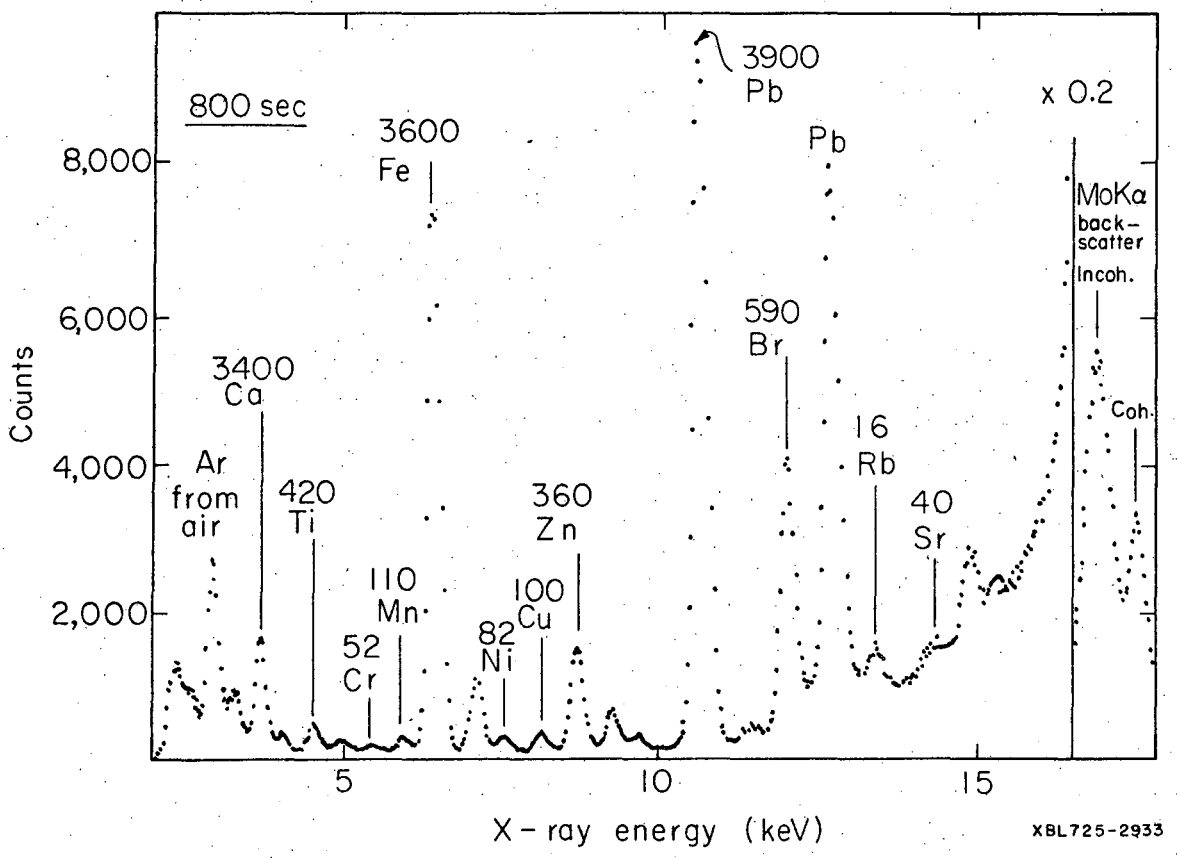
800 sec
3600
Fe
3900
Pb
x 0.2
Pb
MoKα
back-
scatter
Incoh.
590
Br
Coh.
16
Rb
3400
Ca
Ar
from
air
420
Ti
360
Zn
40
Sr
110
Mn
100
Cu
52
Cr
82
Ni
8,000
6,000
4,000
2,000
Counts
5
10
15
X-ray energy (keV)
XBL725-2933

Fig. 16

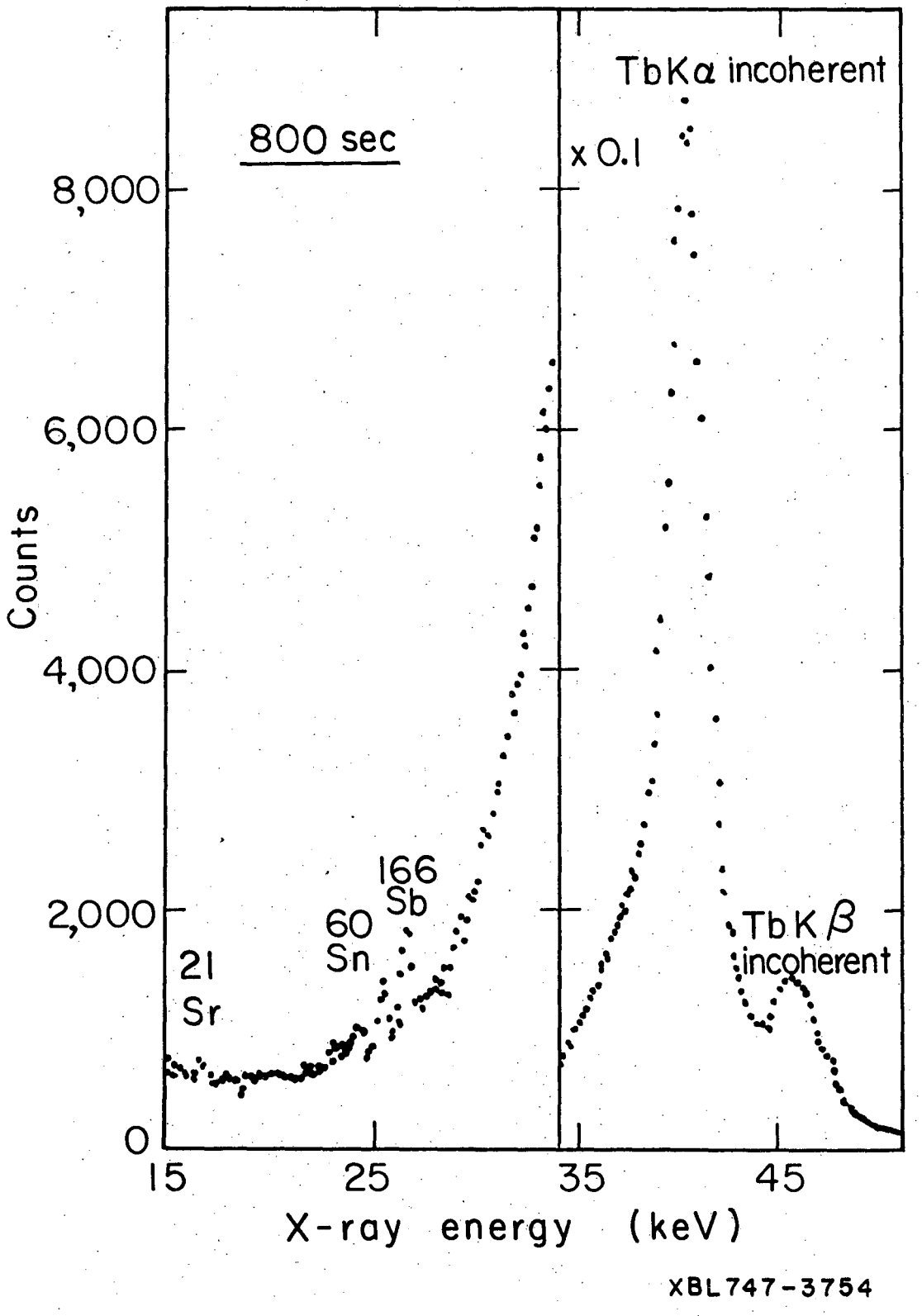
800 sec
x 0.1
TbKα incoherent
8,000
6,000
4,000
2,000
0
Counts
21
Sr
60
Sn
166
Sb
TbKβ
incoherent
15
25
35
45
X-ray energy (keV)
XBL747-3754

Fig. 17

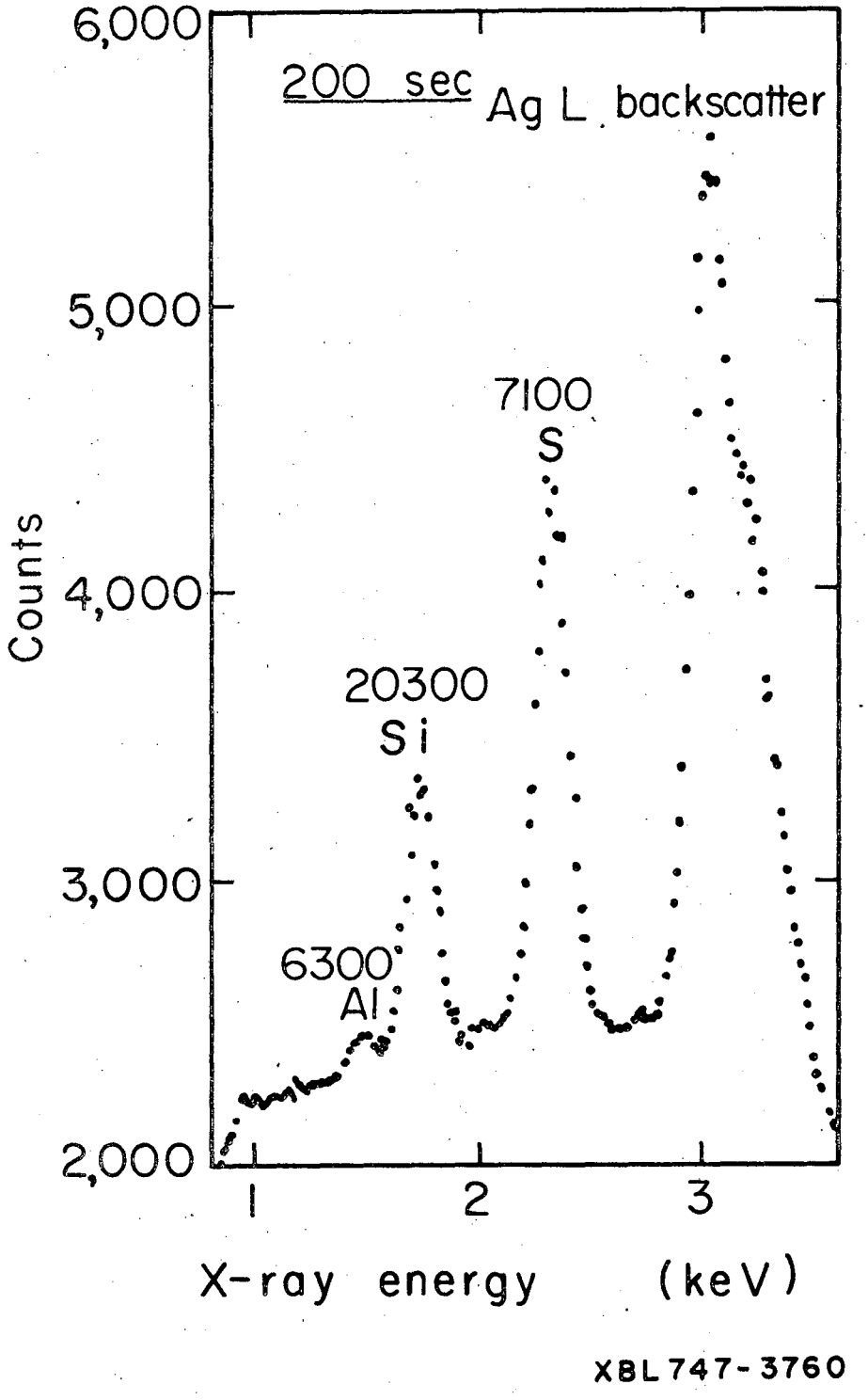
6,000
5,000
4,000
3,000
2,000
Counts
200 sec
Ag L backscatter
7100
S
20300
Si
6300
Al
1
2
3
X-ray energy (keV)
XBL747-3760

Fig. 18

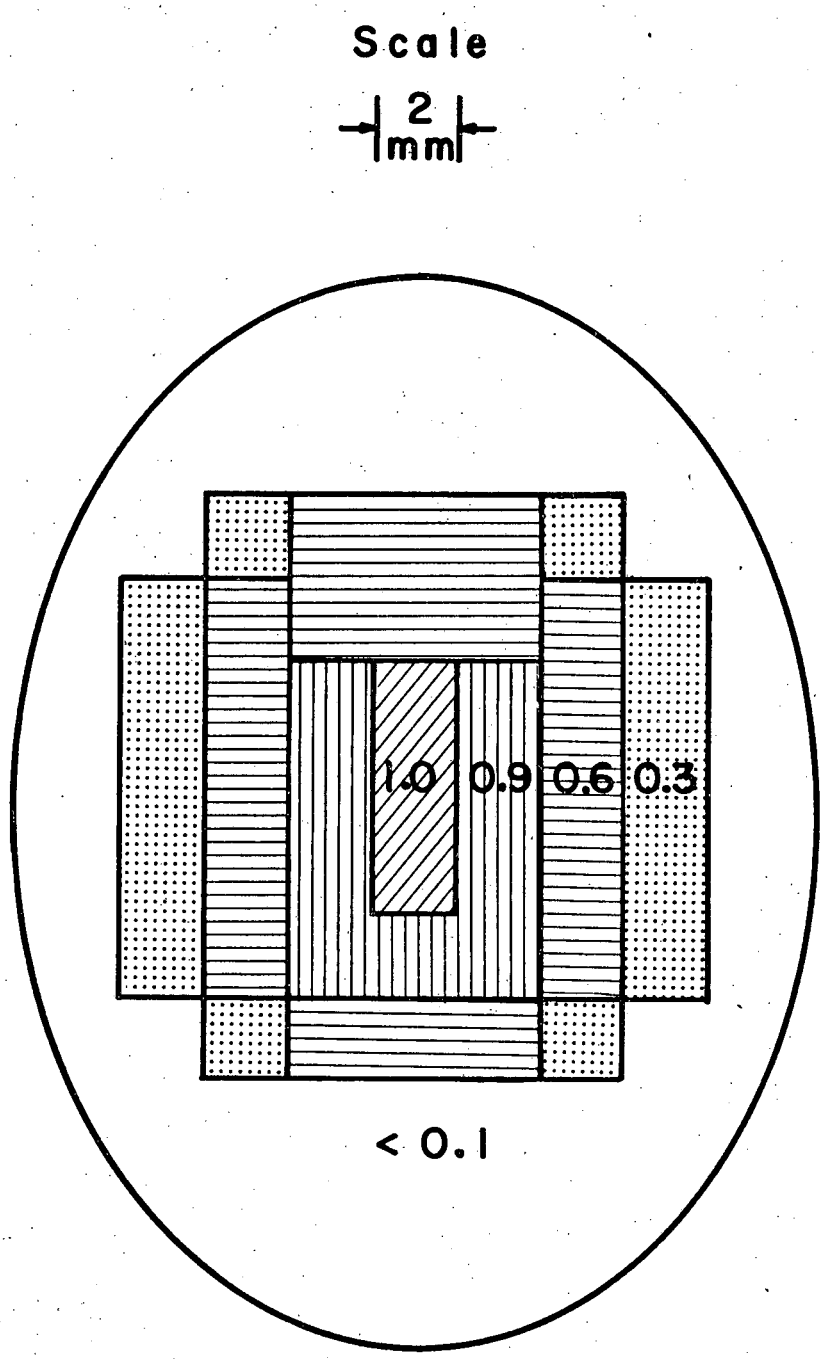

Fig. 19

TECHNICAL INFORMATION DIVISION
LAWRENCE BERKELEY LABORATORY
UNIVERSITY OF CALIFORNIA
BERKELEY, CALIFORNIA 94720